NASA CR-159,156

NASA Contractor Report 159156

Application of an Optimized Wing-Winglet Configuration to an Advanced Commercial Transport

C. A. Shollenberger

McDonnell Douglas Corporation
Douglas Aircraft Company
Long Beach, California 90846

FOR EARLY DOMESTIC DISSEMINATION

NASA

APPLICATION OF AN
OPTIMIZED WING-WINGLET CONFIGURATION
TO AN ADVANCED COMMERCIAL TRANSPORT

November 1979

by

Douglas Aircraft Company

McDonnell Douglas Corporation

Long Beach, California

80N71546

FOREWORD

This document presents the results of a contract study performed for the National Aeronautics and Space Administration (NASA) by the Douglas Aircraft Company, McDonnell Douglas Corporation. This work was part of the Energy Efficient Transport (EET) project of the Aircraft Energy Efficiency (ACEE) program. Specifically, the study was one task in the contract, Selected Advanced Aerodynamic and Active Control Concepts Development. The activity included the preliminary design of an optimized wing-winglet aircraft configuration and comparison of its operating characteristics with an advanced technology conventional wing commercial transport.

ACKNOWLEDGEMENTS

CONTENTS

TABLES

SYMBOLS

The longitudinal aerodynamic characteristics presented in this report are referred to the stability-axis system. Force and moment data have been reduced to coefficient form based on trapezoidal wing area. All dimensional values are given in both International System of Units (SI) and U.S. Customary Units, the principal measurements and calculations using the latter (see Reference 1).

Coefficients and symbols used herein are defined as follows:

A	enclosed area
A_c	area of cover panel
AR	wing aspect ratio
$C_{D_{induced}}$	induced drag coefficient
$C_{D_{parasite}}$	parasite drag coefficient
$C_{D_{total}}$	total aircraft drag coefficient
C_L	lift coefficient
C_{L_A}	aircraft lift coefficient
$C_{L_{max_{basic}}}$	maximum lift coefficient of wing without flap deflection of dynamic effects
$C_{L_{maxV_{min}}}$	maximum lift coefficient at minimum speed
$C_{L_{V_{min}}}$	lift coefficient at minimum unstick speed
$C_{L_{to}}$	tail-off lift coefficient
$C_{L_{V_{mu}}}$	lift coefficient at minimum unstick speed

C_n	winglet normal force coefficient
C_{RBM}	wing root bending moment
C_s	box structural chord
I	bending stiffness
I_7	wing bending rigidity of configuration WW7
J	torsional stiffness
J_7	wing torsional rigidity of configuration WW7
$L/D_{trimmed}$	trimmed lift-to-drag-ratio
M	limit vertical bending moment about elastic axis
S	area of wing
U_{de}	gust velocity
V_{DIVE}	dive speed
V_F	flutter speed
WW	wing-winglet configuration designation
X_{EA}	elastic axis stations
b	span of wing
c	airfoil chord
e	induced drag efficiency factor
Fc_{ult}	estimated typical compression allowable
Fe	equivalent allowable stress
h	one-half of thickness
l	winglet spanwise length
s	spanwise distance along winglet
t	maximum airfoil thickness

x	streamwise coordinate
y	spanwise coordinate
z	vertical coordinate
α	angle of attack
α_i	wing section incidence angle
$\Delta C_{D_{compressibility}}$	drag coefficient resulting from fluid compressibility
$\Delta C_{D_{trim}}$	drag coefficient resulting from trimming aircraft moments
$\Delta C_{L_{FLAP}}$	flap incremental lift coefficient
$\Delta C_{L_{max_{flap}}}$	increment in maximum lift coefficient resulting from deflection of trailing edge flap
$\Delta C_{L_{max_{VCK}}}$	increment in maximum lift coefficient resulting from deflection of variable camber Krueger flap
$\Delta C_{L_{trim}}$	increment in lift coefficient resulting from trimming aircraft moments
$\Delta C_{L_{V_{min}}}$	increment in lift coefficient resulting from dynamic deceleration of aircraft
ΔC_m	incremental pitching moment coefficient
$\Delta\Delta C_{D_i}$	difference between wing-winglet and baseline aircraft incremental flap drag coefficient
ΔX_{EA}	span increments between X_{EA} stations
δ_F	flap deflection
$\delta_{f_{eff}}$	effective flap deflection
δ_{SP}	spoiler deflection
η	nondimensional spanwise location
ω	bending material weight

SUMMARY

This report presents the design of an aircraft which from the initial conceptual stages employs an integrated wing and winglet lift system. Comparison was made with a conventional baseline configuration employing a high-aspect-ratio supercritical wing. An optimized wing-winglet combination was selected from four proposed configurations for which aerodynamic, structural, and weight characteristics were evaluated. Each candidate wing-winglet configuration was constrained to the same induced drag coefficient as the baseline aircraft. The selected wing-winglet configuration was resized for a specific medium-range mission requirement, and operating costs were estimated for a typical mission. Study results indicated that the wing-winglet aircraft was lighter and could complete the specified mission at less cost than the conventional wing aircraft. These indications were sensitive to the impact of flutter characteristics and, to a lesser extent, to the performance of the high-lift system. Further study in these areas is recommended to reduce uncertainty in future development.

INTRODUCTION

The aerodynamic ramifications of nonplanar wing configurations have long been known and they have often been suggested as a technique for reduction of aerodynamic induced drag. However, since a wing tip extension is always aerodynamically more efficient than a comparably sized nonplanar configuration, wing tip devices have rarely been applied to transport aircraft. Nevertheless, when the aerodynamic benefits of wing tip devices are considered in combination with structural aspects and physical constraints (e.g., maximum wing span feasible for existing ramp facilities), the nonplanar wing configuration becomes a more attractive candidate for transport aircraft. R. T. Whitcomb (References 2, 3, and 4) has recently developed and refined the application of wing tip devices which have been named "winglets." The winglet (a small, nearly vertical, winglike surface) effectively increases the span of a conventional wing but additionally is carefully tailored to carry the requisite aerodynamic loading without significant viscous or compressibility interference at cruise Mach numbers.

The majority of winglet development efforts have been oriented toward modification of existing aircraft to enhance their capabilities and performance. The effectiveness of a wing tip modification, either tip extension or winglet, in a retrofit application is controlled by the existing aerodynamic and structural characteristics of the configuration. For example, winglet induced drag reduction potential is directly influenced by the magnitude of wing tip loading, and similarly, structural capabilities of a particular wing may significantly influence the choice and size of the tip device. Although winglets appear to be a viable device for a retrofit application, the use of an existing wing complicates and restricts the potential gains which are achievable.

1

In contrast to the retrofit concept where aerodynamic loading and structural properties of an existing wing strongly influence any wing-winglet design, the present study considered the develpment of an advanced commercial aircraft which from the outset was designed to employ a wing and winglet operating in conjunction with each other as a unified lifting system. In order to simplify the evaluation of various wing-winglet conbinations, the aerodynamic characteristics of each configuration were constrained to the same values as for the baseline airplane and the "optimum" constrained wing-winglet was the one chosen solely on the basis of mimimum structural weight. This approach facilitated structural and aerodynamic design of the wing-winglet combination as a system rather than as a remedial device attached to a wing initially intended to operate independently. Therefore, a more effective exploitation of the winglet concept should be possible. The objective of the present study was to evaluate the benefits of an advanced commercial transport with a wing-winglet (optimized within the constraints stated below) in relation to one with a conventional wing design.

The design and configuration selection process has been conducted for mission requirements regarded as typical for a large and important class of aircraft. The conventional aircraft was based on thorough investigation and definition in separate Douglas Aircraft Company studies. Included in the wing-let configuration selection process were aerodynamic analysis, structural design (including allowance for maneuver capability, gust loads, and adequate flutter margin), and weight estimation for a series of parametrically selected candidate wing-winglet combinations. The best wing-winglet configuration was then selected for sizing and performance evaluation so that the operating characteristics could be estimated and compared with those of the conventional baseline aircraft.

Evaluation of the conventional baseline and wing-winglet aircraft was based primarily on direct operating costs, but other parameters such as fuel use were also examined.

The basic mission requirements for which both the wing-winglet configuration and conventional baseline aircraft were designed are given in Table 1. The mission used in evaluating the aircraft consisted of the 1389-kilometer (750-nautical-mile) trip specified in Table 2, and represents a typical application of an aircraft designed to the requirements of Table 1. The baseline aircraft is shown in Figure 1 and its geometric characteristics are given in the table insert of the figure. The baseline aircraft was the DC-X-200 commercial passenger transport which was envisioned as a derivative of the DC-10 aircraft. The baseline aircraft featured a shortened DC-10 fuselage of 230-seat nominal capacity. Aerodynamic features of the DC-X-200 included a high-aspect-ratio planform wing with supercritical airfoils. The high-lift system consisted of a full-span variable camber Krueger leading-edge flap and an 80-percent span high-extension two-segment flap. The configuration included a longitudinal stability augmentation system that allowed operation at a center-of gravity range aft of that of an unaugmented aircraft.

Table 1
AIRCRAFT MISSION REQUIREMENTS

Payload	21,390 kilograms (47,150 pounds) (230 passengers and baggage)
Range	5844 kilometers (2620 nautical miles) equivalent still air distance
Initial Cruise Altitude	10,363 meters (34,000 feet)
Initial Cruise Mach Number	0.80
Approach Speed	241 kilometers/hour (130 knots) or less

Specified Engines GE CF6-45; field length not specified.

CHARACTERISTICS DATA				
	WING		HORIZONTAL	VERTICAL
ITEM	REF	ADJUSTED	TAIL	TAIL
AREA, SQ FT	2175	2367.4	682	405.
ASPECT RATIO	10.85	9.97	3.8	1.6
TAPER RATIO	.1407	(.250)	.35	.35
SWEEP DEG, C/4	30°		30°	35°
DIHEDRAL, C/4	+4°		+10°	~
TAIL VOLUME	~		1.13	~

PAYLOAD CAPACITY ~

● FIRST CLASS   = 6 ABREAST AT 38 IN. PITCH =   20 (8.7%)
   TOURIST CLASS = 9 ABREAST AT 34 IN. PITCH = 210 (91.3%)
   TOTAL = 230 SEATS

● UPPER (CONVENTIONAL) GALLEYS

● CARGO VOLUME ~

   FORWARD BAY = 8 LD-3 CONTAINERS AT 158 FT^3 = 1264 FT^3
   CENTER BAY   = 10 LD-3 CONTAINERS AT 158 FT^3 = 1580 FT^3
   AFT BAY   = BULK   =   510 FT^3
   TOTAL = 3354 FT^3
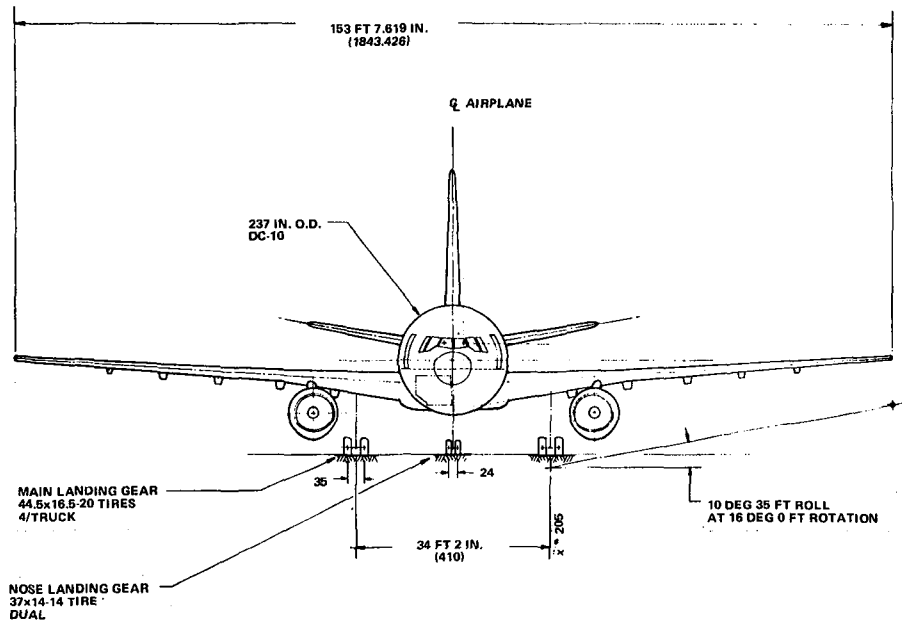
FIGURE 1. BASELINE ADVANCED COMMERCIAL TRANSPORT
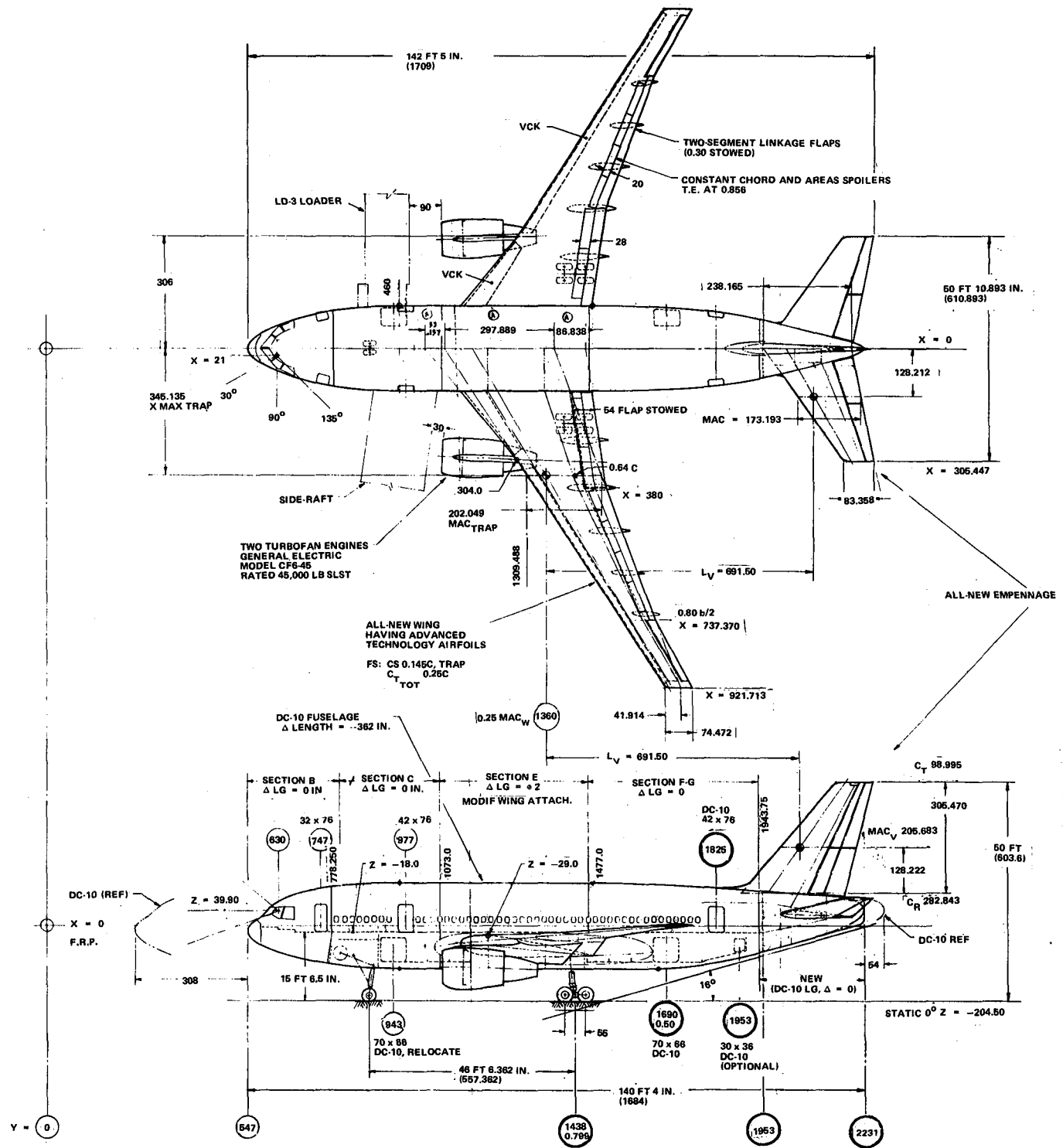
FIGURE 1. BASELINE ADVANCED COMMERCIAL TRANSPORT (CONCLUDED)

5

Table 2

TYPICAL MISSION PROFILE

Flight Segment	Requirements
Taxi Out	5 minutes at taxi thrust
Take Off	Climb to 457 meters (1500 feet)
Climb	Maximum climb thrust, long range climb schedule to initial cruise altitude
Cruise	Constant Mach number, step cruise technique (31,000, 35,000, 39,000 feet) 1389 kilometer (750 nautical mile) mission at best constant odd altitude
Descent	Employ long range speed schedule to sea level
Approach	4 minutes at approach thrust
Taxi In	3 minutes at taxi thrust

Reserve fuel based on FAR 121.639 as follows:

Climb from sea level to 9144 meters (30,000 feet) using maximum climb thrust and long range speed schedule, cruise at 9144 meters (30,000 feet) at 99 percent maximum specific range, descend to sea level for total distance to alternate of 370.4 kilometers (200 nautical miles) and cruise for 45 minutes at 9144 meters (30,000 feet) at 99 percent maximum specific range.

During the wing-winglet configuration selection phase of the study, the basic aerodynamic capability of the baseline aircraft was maintained for all candidate wing-winglet configurations and therefore the merit of each configuration was measured solely by weight saving relative to the baseline. This procedure of conserving the baseline aircraft aerodynamic characteristics employs the baseline lift/drag design point and eliminates a substantial number of stages from the wing-winglet design process that would be required without

use of the baseline aircraft as a starting point. Basic aerodynamic character-
istics which were conserved include induced drag coefficient, compressibility
drag effects, cruise lift coefficient, lateral aircraft stability, buffet
margin, and high-lift capability.

SELECTION OF WING-WINGLET CONFIGURATION

Most of the present study effort involved the determination of an optimum
(within the practical constraints of a preliminary feasibility study) wing-
winglet configuration. As a basis for the optimization, a series of wing-
winglet configurations was designed with essentially identical aerodynamic
characteristics so that they could be judged on their weight. The weight
estimation was supported by structural strength and stiffness analyses,
including the impact of flutter. An alternative design approach, maintaining
fixed weight and evaluating configurations based on aerodynamic improvement,
could have been applied to obtain an "optimum" wing-winglet combination.
However, this alternative was beyond the scope of the study.

Wing Design Rules

Since it was desired to match the basic performance characteristics of
the baseline aircraft with each wing-winglet design, a series of rules was
derived to ensure that all designs were aerodynamically equivalent. No
transonic flow calculations were feasible for the nonplanar winglet configura-
tions, and consequently, to preserve the impact of compressibility effects on
the lift-system performance, certain baseline geometric characteristics were
maintained for the winglet design.

The first rule required that the induced drag coefficient of the winglet
configuration match the baseline value. As will be shown later, the assump-
tion of equal induced drag implied a wing span length for a given drag
efficiency factor. The second rule required the trapezoidal wing area of
each wing-winglet configuration to be the same as that of the baseline wing.
This rule ensured nearly constant cruise lift coefficients for all configura-
tions since the gross weights of the baseline and wing-winglet configuration

9

were not expected to differ significantly. Subsequent to the wing-winglet configuration selection, a resizing of the aircraft was performed to determine the final wing area.

In an attempt to maintain the transonic cruise capability of the baseline wing, the baseline leading edge sweep of 32.9 degrees and trailing edge sweep of 20.3 degrees were applied to the winglet configurations. Additionally, the baseline aircraft supercritical airfoil sections were identically employed on the wing-winglet planform with corresponding aerodynamic definition points as shown in Figure 2. Furthermore, the inboard leading edge extension (located
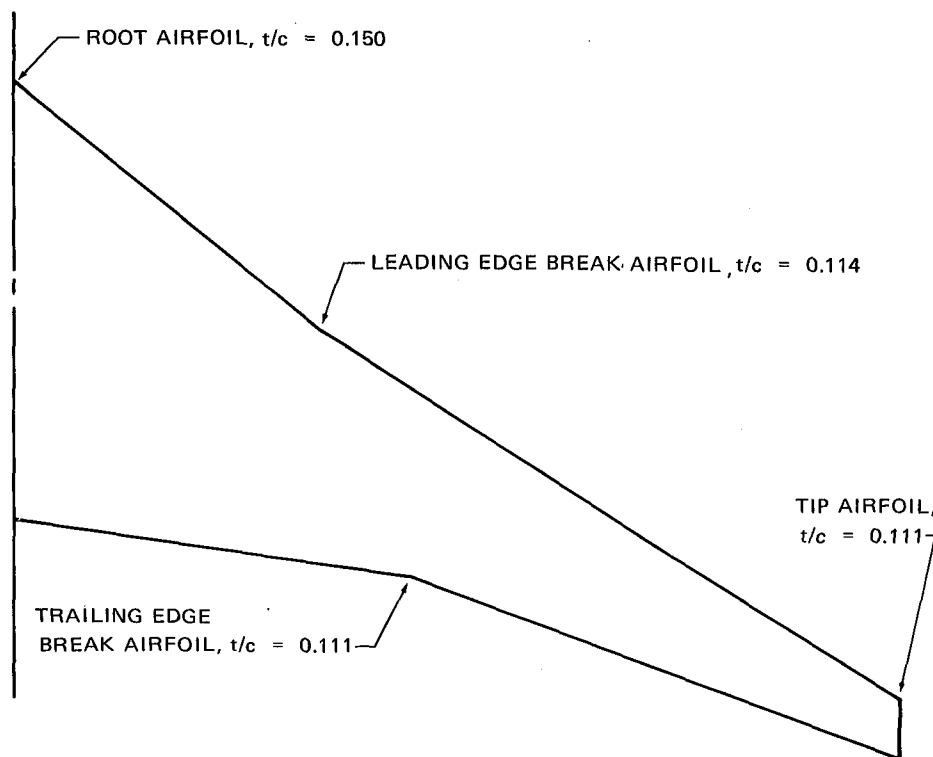
FIGURE 2. AIRFOIL DEFINITION FOR WING-WINGLET CONFIGURATION

10

between the pylon location of 7.72 meters [304 inches] and the root) of the baseline wing was employed in the wing-winglet combinations. The leading edge extension was intended to maintain swept isobars on the inboard panel of the wing at cruise Mach numbers. This configuration has been shown in previous studies (reported in Reference 5) to provide significant improvement over a straight leading edge for the baseline wing. The inboard leading-edge extension tapers from 10 percent of the trapezoidal chord at the wing root to zero at the pylon location.

An important physical constraint which must be imposed on any practical configuration is adequate provision for the main landing gear in the retracted position. The gear pivot location was specified to be at a spanwise distance of 5.59 meters (220 inches) outboard of the wing root and 0.38 meter (15 inches) forward of the 0.666 mean aerodynamic chord point. In order to provide storage for the gear, an inboard wing trailing edge extension was required which passed through a point 1.96 meters (77 inches) aft of the gear pivot point. A sketch of the geometric requirements of the wing for gear storage is given in Figure 3. Geometric requirements for locating and housing the landing gear were derived from Douglas Aircraft Company studies of the baseline aircraft.

The third wing design rule specified a wing dihedral angle of 4 degrees for lateral stability requirements. Since the winglet is a dihedral surface, this could increase the lateral stability of the configuration beyond the baseline value.

The above wing specifications define the wing except for the span which is determined by the induced drag efficiency level.

10% TRAPEZOIDAL CHORD

7.72 M (304 IN.)

66.6% MAC — 0.38 M (15 IN.)

GEAR LOCATION

8°

5.59 M (220 IN.)

POINT 1.96 M (77 IN.) AFT OF GEAR LOCATION THROUGH WHICH TRAILING EDGE EXTENSION PASSES
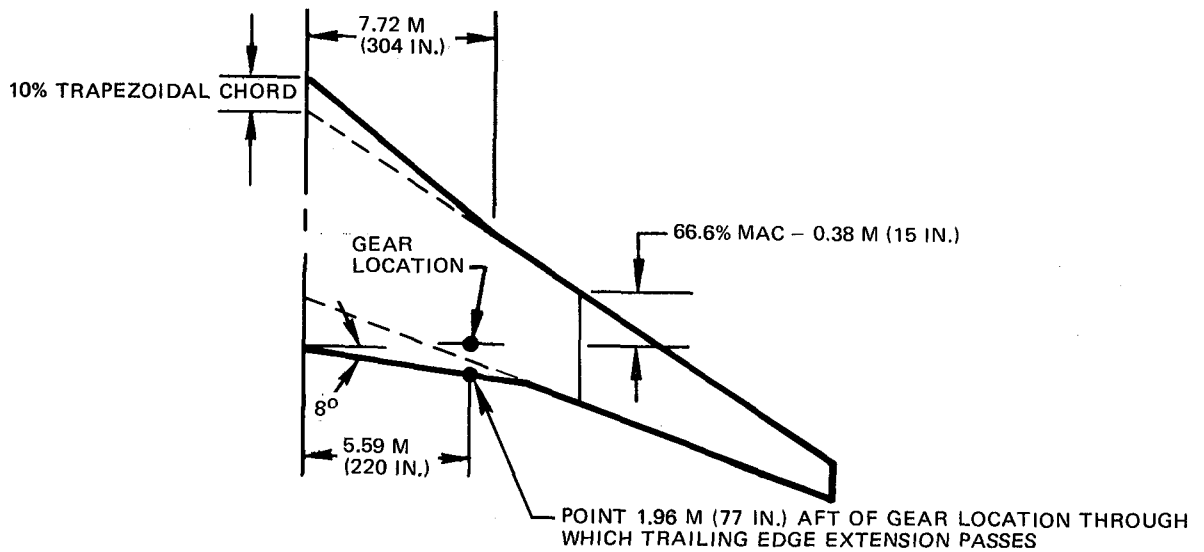
FIGURE 3. ILLUSTRATION OF WING PLANFORM DESIGN RULES

Winglet Design Rules.

A set of design specifications, similar to those developed for the wing design, based on NASA development programs and Douglas Aircraft Company experience, was prescribed for the upper surface winglet design. Since no wind tunnel test of the final configuration was feasible in the current study, it was decided that conservative design rules based on proven results should be employed. Therefore the winglets of each design were basically modeled after the successful application of Reference 2. In Reference 2, a winglet dihedral of 75 degrees and a winglet taper ratio of 0.3 were employed. Additionally, the midchord sweep of the wing and winglet were equated, and the wing tip trailing edge and winglet root trailing edge were kept coincident to avoid superposition of wing-winglet velocity peaks. The span of the winglet was based on the span of the wing since span ratio appeared to be an appropriate scaling for maintaining the induced drag effectiveness of the NASA Whitcomb configurations. The span of all winglets was 14.8 percent of the wing semispan. As a result of the cooperative NASA/Douglas Aircraft Company

12

wind tunnel tests, which are reported in Reference 6, it was decided to employ a winglet root chord of 77 percent of the wing tip chord in contrast to the earlier Whitcomb value of 65 percent. The increased winglet chord reduced the section normal force coefficient of the winglet to values which could be achieved without aerodynamic buffet. The airfoil section selected for the winglet is the NASA modified General Aviation-type airfoil of Table 3. This airfoil has been employed effectively in previous winglet applications, including those reported on in References 2 and 6.

Early in the study it was decided to employ only an upper-surface winglet, primarily for simplicity. It was assumed that a lower winglet could be incorporated in more refined designs. From previous experience it was presumed that the lower winglet would produce an additional benefit and hence it was believed that its omission represented design conservatism.

Aerodynamic Design

As previously mentioned, the design procedure implied that all benefits of the incorporation of a winglet in the lift system design would be realized in weight reductions while the aerodynamic characteristics were conserved. This philosophy facilitated a practical configuration selection without the exhaustive design study required for an entirely new design. This simplification did not significantly restrict the design since the optimized wing-winglet configuration was resized for the evaluation.

Wing-Winglet Planform Specification. — The wing and winglet design rules described earlier were sufficient to completely specify a configuration except for the most significant parameter — span. Therefore, a series of wing-winglet

Table 3

AIRFOIL COORDINATES FOR WINGLETS

x/c	z/c for -	
	Upper Surface	Lower Surface
0.0	0.0	0.0
0.0020	0.0077	-0.0032
0.0050	0.0119	-0.0041
0.0125	0.0179	-0.0060
0.0250	0.0249	-0.0077
0.0375	0.0296	-0.0090
0.0500	0.0333	-0.0100
0.0750	0.0389	-0.0118
0.1000	0.0433	-0.0132
0.1250	0.0469	-0.0144
0.1500	0.0499	-0.0154
0.1750	0.0525	-0.0161
0.2000	0.0547	-0.0167
0.2500	0.0581	-0.0175
0.3000	0.0605	-0.0176
0.3500	0.0621	-0.0174
0.4000	0.0628	-0.0168
0.4500	0.0627	-0.0158
0.5000	0.0618	-0.0144
0.5500	0.0599	-0.0122
0.5750	0.0587	-0.0106
0.6000	0.0572	-0.0090
0.6250	0.0554	-0.0071
0.6500	0.0533	-0.0052
0.6750	0.0508	-0.0033
0.7000	0.0481	-0.0015
0.7250	0.0451	0.0004
0.7500	0.0419	0.0020
0.7750	0.0384	0.0036
0.8000	0.0349	0.0049
0.8250	0.0311	0.0060
0.8500	0.0270	0.0065
0.8750	0.0228	0.0064
0.9000	0.0184	0.0059
0.9250	0.0138	0.0045
0.9500	0.0089	0.0021
0.9750	0.0038	-0.0013
1.0000	-0.0020	-0.0067

combinations with varying spans was designed to have nearly equivalent aerodynamic characteristics (in particular the same induced-drag coefficient) as the baseline aircraft.

Maintaining constant induced drag at a specified lift while varying the configuration span required a variety of spanwise load distributions among the competing designs. A minimum span exists for the wing-winglet combination beyond which the required induced drag cannot be maintained. At this minimum span the wing-winglet combination is loaded for its minimum induced drag. At spans greater than the minimum value, the spanwise distribution of load may be altered from that for minimum induced drag in a manner that is advantageous from a structural viewpoint.

Figure 4 presents the relationship between wing root bending moment ratio and drag efficiency factor for an isolated planar wing and the appropriate wing-winglet combination. The adherence to the baseline-induced drag for all wing-winglet combinations of different spans required variation of the span-wise aerodynamic load distribution. The proper loading which resulted in the desired drag value was determined by employing the numerical method of Reference 7. This method analyzes the wing-winglet configuration in the far downstream field (Trefftz plane), and predicts minimum induced-drag aerody-namic loadings subject to root bending moment and other optional constraints. Using this method, the root bending design points of Figure 4 were employed as input constraints and the optimum loadings were calculated for each wing-winglet configuration. Aerodynamic loadings for the winglets were obtained simultaneously with the wing-load distributions.
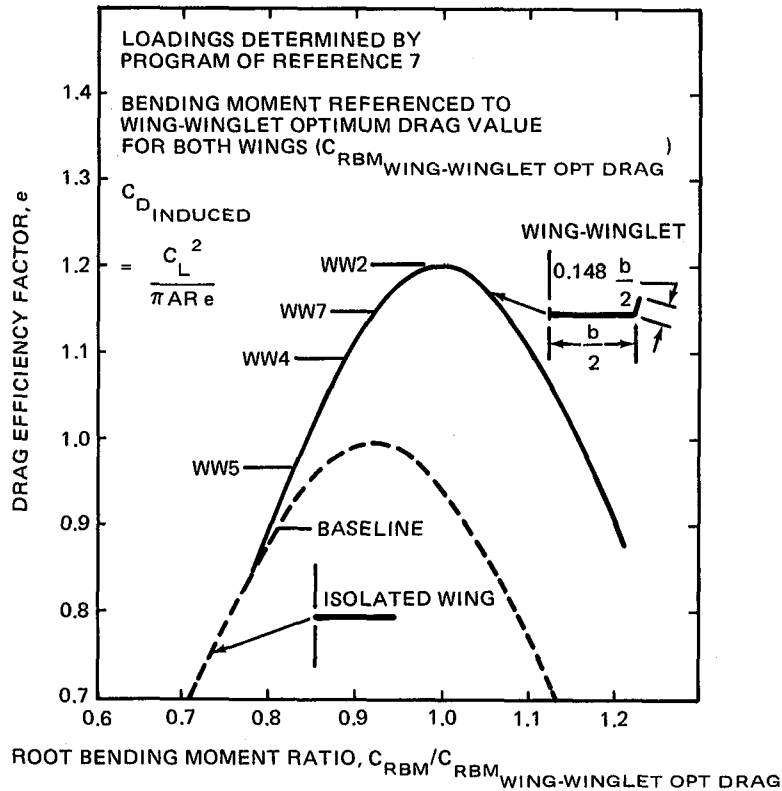
FIGURE 4. DRAG FOR SPECIFIED ROOT BENDING MOMENT

Wing root bending moment is probably the best single parameter for eval-uating the impact of aerodynamic loading on wing structural weight. Higher root bending moments generally imply higher wing weights, but of course detailed structural analyses are required to quantify the weight impact. Drag efficiency factor, e, is a simple way of expressing the level of inviscid induced drag relative to the minimum induced drag for a given lift system so that

$$e = \frac{\text{minimum possible induced drag}}{\text{actual induced drag}}$$

(1)

$$e = \frac{C_L^2}{C_{D_{induced}} \pi AR}$$

16

Therefore, the lift-induced drag coefficient (ignoring twist drag) can be expressed in terms of the efficiency factor as

$$C_{D_{induced}} = \frac{C_L^2}{\pi ARe} \qquad (2)$$

where C_L is the aircraft lift coefficient and AR is the wing aspect ratio, b^2/S.

Classical lifting line theory predicts a maximum value of the efficiency factor of 1.0 for a planar wing whereas nonplanar configurations, such as wing-winglet combinations, may achieve maximum efficiency factors greater than 1.0 (if the minimum induced drag is based on the span of the wing without the winglet). For a conventional planar wing, the optimum aerodynamic-structural-weight design point is usually at a drag efficiency factor which is a few percentage points less than the maximum value. By analogy, it was anticipated that the optimum design point for a wing-winglet combination would be somewhat less than the maximum value. This maximum value (1.21) was predicted independently by the methods of References 7 and 8.

Figure 4 indicates that, except at the maximum drag efficency condition, two root bending moment values exist for each drag efficiency value. Normally only the lower value of root bending moment would be of interest since the higher root bending moment implies unnecessary weight penalty with no aerodynamic benefit. Four configurations, ranging from the aerodynamic optimum to 20-percent reduction from optimum in efficiency factor, were selected for detailed aerodynamic-structural-weight design, analysis, and evaluation. These four cases are indicated in Figure 5 as WW2, WW4, WW5, and WW7.

The spans of the various configurations were uniquely determined from the specification of the drag efficiency factor since the induced-drag coefficient

19.92 M (784.3 IN.) WW2B
20.40 M (803.3 IN.) WW7
20.97M (825.5 IN.) WW4
22.19 M (873.5 IN.) WW5
23.41 M (921.7 IN.) BASELINE WING
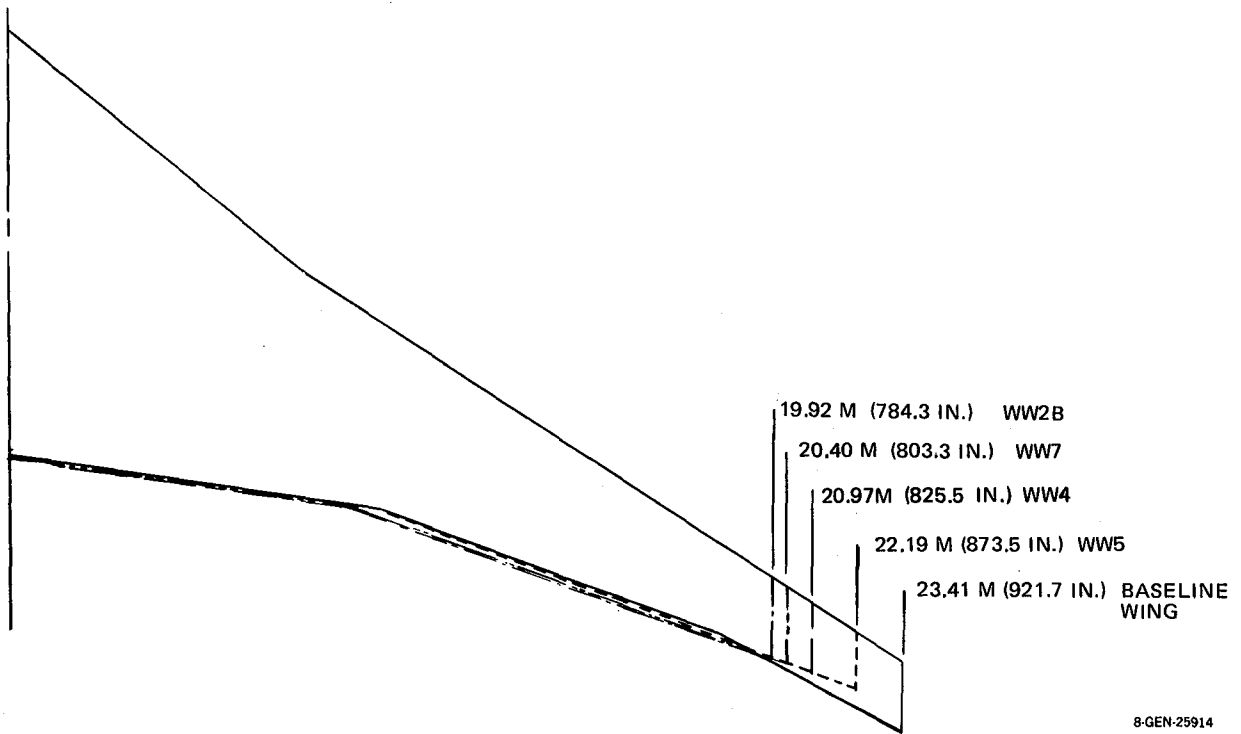
8-GEN-25914

FIGURE 5. PLANFORMS FOR WING-WINGLET OPTIMIZATION

was conserved at the design lift coefficient for all designs. From Equation 2, the wing aspect ratio can be determined as

$$AR = \frac{C_L^2}{\pi e \, C_{D_{induced}}} \qquad (3)$$

and, consequently, the wing span is given by

$$b = \frac{C_L \sqrt{S}}{\sqrt{\pi e \, C_{D_{induced}}}} \qquad (4)$$

where S is the reference wing area.

The design lift coefficient was 0.60 and the baseline reference area of 202.1 square meters (2175 square feet) was initially applied to all configurations. Therefore, the span of any configuration could be determined from Equation 4 where the drag efficiency factor and baseline drag coefficient, $C_{D_{induced}}$, was known.

18

Applying Equation 4 and the wing-winglet design rules described previously
yielded the wing planforms of Figure 5 for the design points illustrated in
Figure 4. The wing-winglet planforms are contrasted with the baseline wing
planform in Figure 5. All planforms conform to the rule specifying the
trapezoidal wing area. Note that the outboard trailing edge break of the
baseline wing has been eliminated. The function of this break was to smooth
the inboard trailing edge break. Since the wing-winglet planforms were of
lower geometrical aspect ratio, the outboard break was not required. Winglet
geometry is exemplified in Figure 6. According to the winglet design rules,
the individual configuration winglets are scaled relative to the wing span;
therefore, each winglet design is unique.
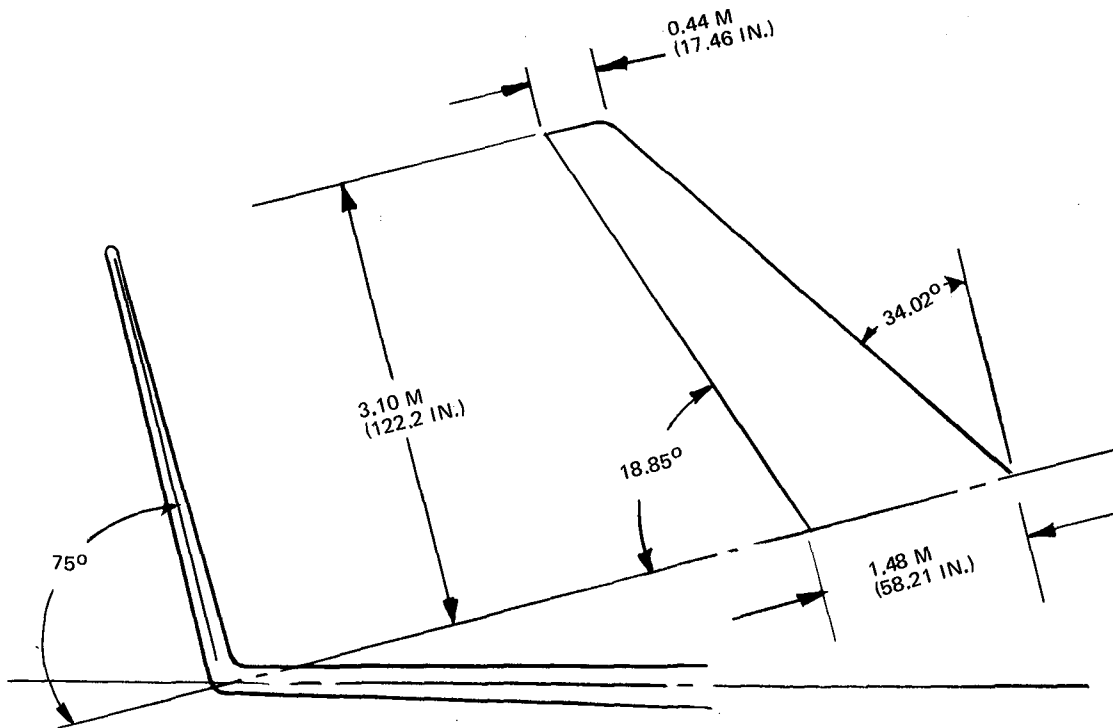
FIGURE 6. WINGLET PLANFORM FOR WING-WINGLET COMBINATION WW4

8-GEN-25861

Spanwise Loading. — As previously mentioned in the foregoing paragraph, the minimum induced-drag aerodynamic load distribution was predicted by use of the numerical method of Reference 6. The discussion also identified the root bending moment design points.

The spanwise lift distribution for four wing-winglet configurations that were selected for study is shown in Figure 7. Typically, the shorter-span configurations have higher tip loadings and therefore higher root bending moments. In addition to the impact of high outboard lift coefficients (which are characteristic of the short span configurations) on root bending moment, the higher lift coefficients may also cause premature buffet onset. In fact, the tip section lift coefficient of wing-winglet configuration WW2 was judged to the unacceptable from the buffet viewpoint and, consequently, this configuration was eliminated from consideration. Configuration WW7 was the shortest span configuration with outboard lift coefficients equivalent to those of the baseline aircraft.

Wing-Winglet Twist Distribution. — In order to obtain the desired wing and winglet loadings, the finite-element lifting surface analysis of Reference 9 was employed to design the twist distribution for both wings and winglets. This method, applied in its design mode, represents each aerodynamic surface by a mean plane and divides each surface into numerous elements. Each analysis element is represented by an elementary vorticity distribution (EVD) and a control point is employed on each element at which a tangential flow condition is imposed.
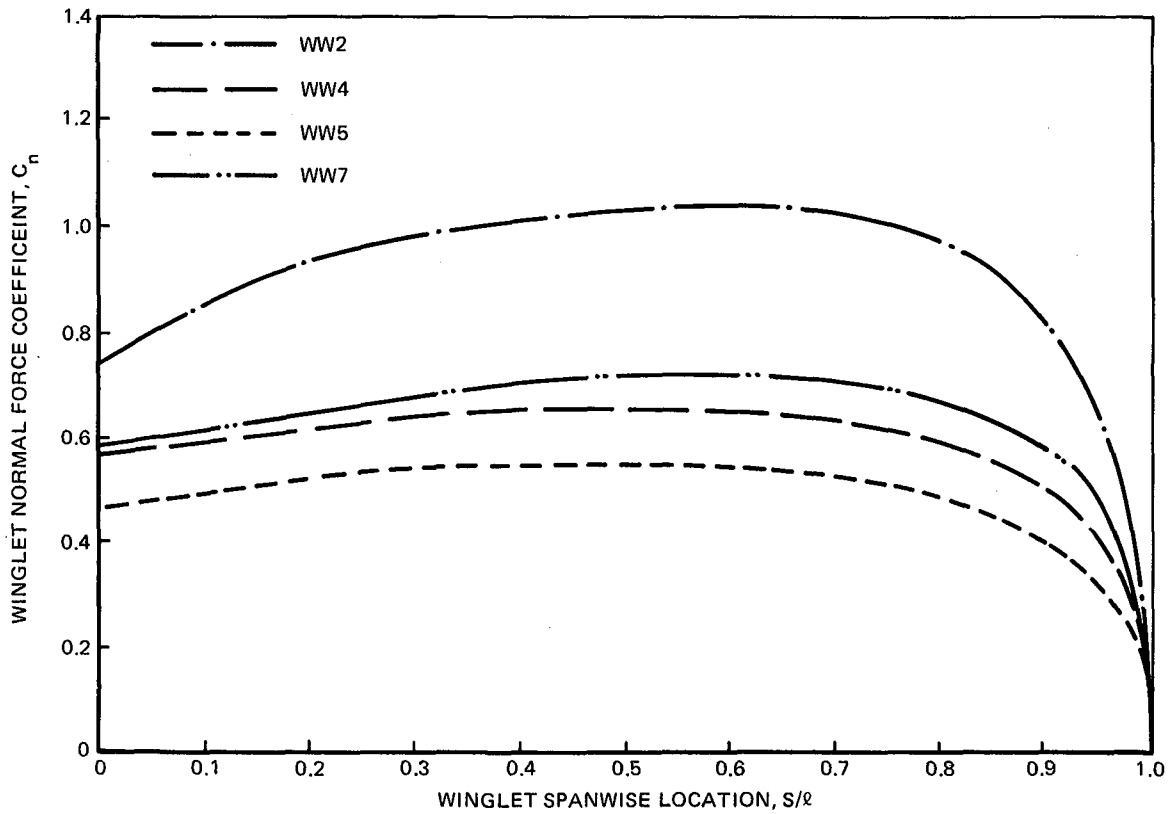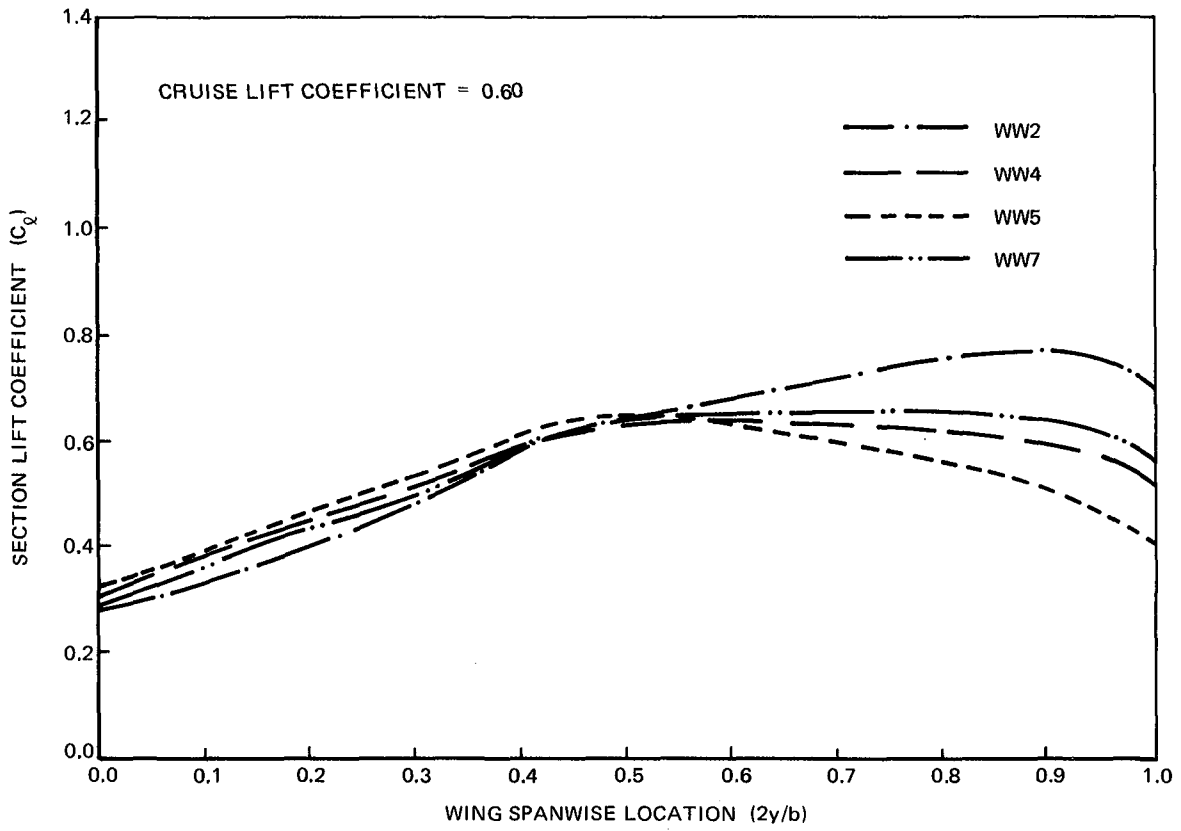
FIGURE 7. WING AND WINGLET SPANWISE LIFT DISTRIBUTION FOR WING-WINGLET DESIGNS

The method employs as inputs airfoil section camber lines, the wing-winglet planforms of Figure 5, and corresponding loadings of Figure 7 to calculate the required twist for each wing and winglet. Example wing and winglet twist distributions are shown in Figures 8 and 9, respectively, for the WW7 configuration. In most cases, some manual adjustment to the predicted twist was required to actually obtain the desired loading for both wing and winglet surfaces. The manual adjustments were necessitated by the linearizations and planar approximation made using the method of Reference 9 in the design mode.

Analysis of Wing-Winglet Configurations. — Each wing-winglet configuration, including the associated twist distributions and airfoil cambers, was evaluated by application of the method of Reference 9 applied in the analysis mode. A major objective of the analysis was verification of the induced-drag value at the design lift coefficient where the intent was to match the baseline aircraft induced-drag coefficient value. A secondary objective was derivation of aerodynamic loads for input to the structural design process. This analysis was required to verify the aerodynamic characteristics of each wing-winglet combination since the method of Reference 9 in the design mode employs small angle approximations and planarizations whereas the analysis mode is not limited to small angles and is nonplanar. Additionally, the analysis mode of the method of Reference 9 has previously been employed successfully to predict winglet performance. It was concluded that the
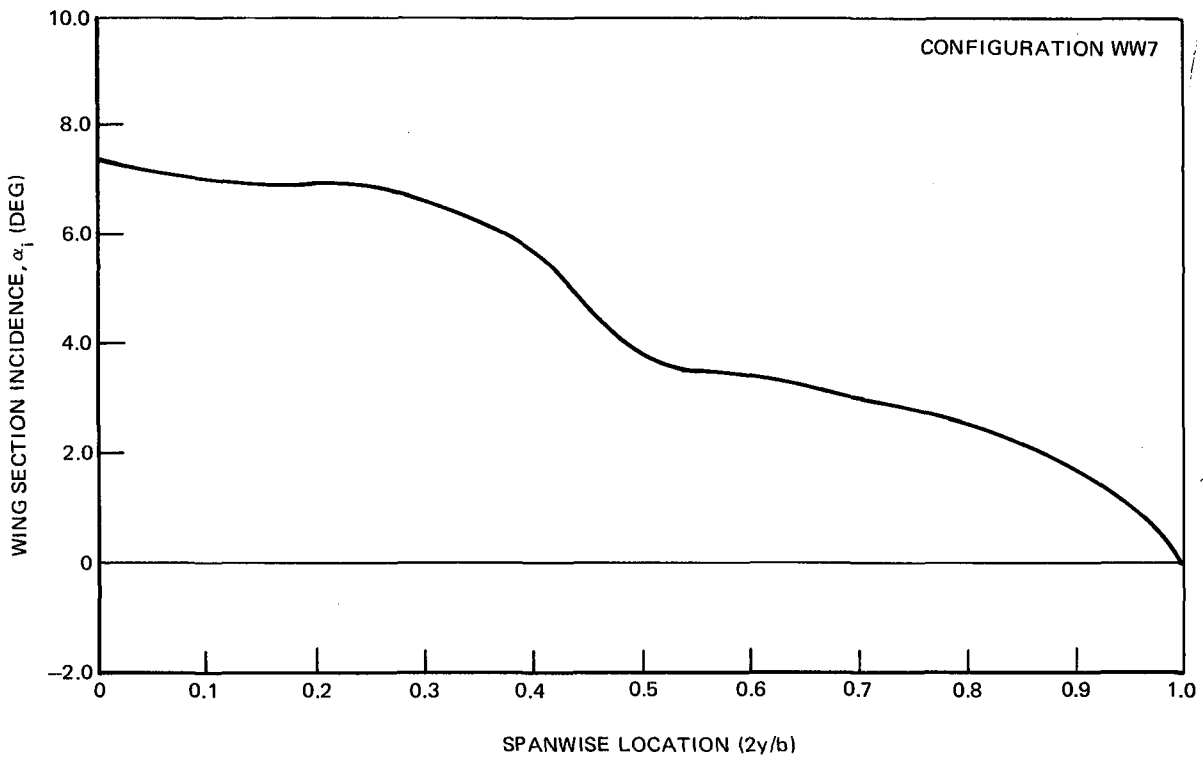
FIGURE 8. WING TWIST
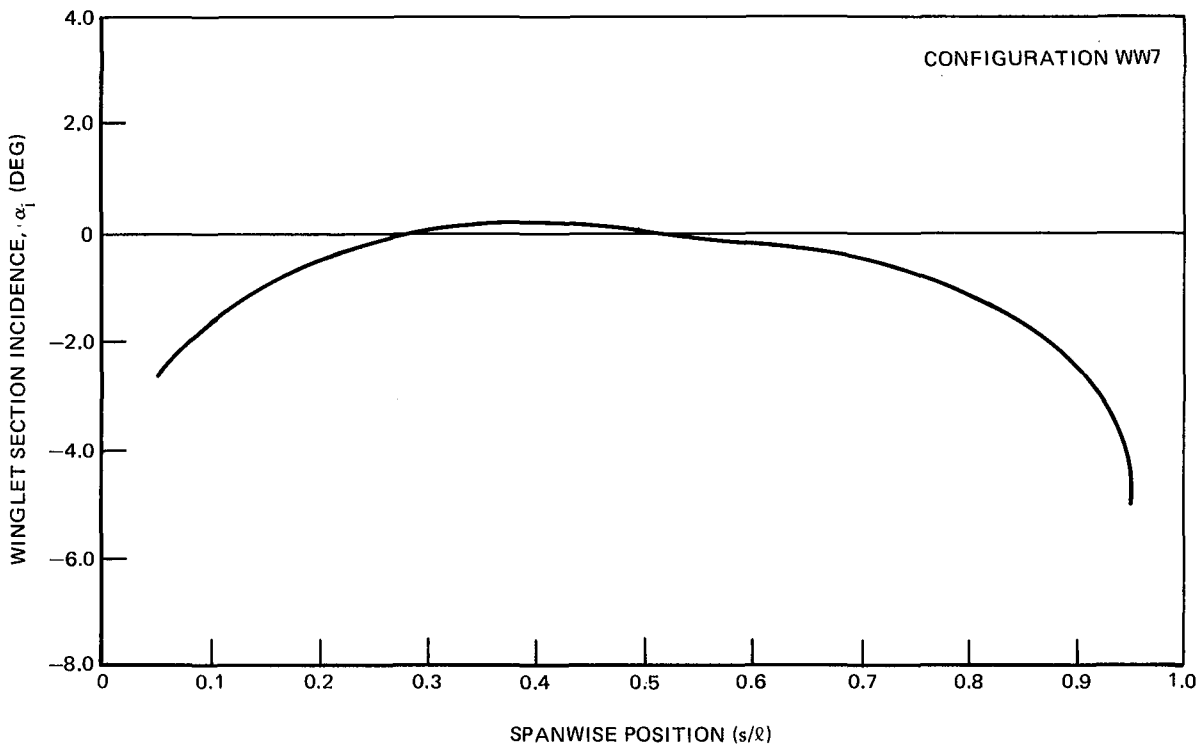
FIGURE 9. WINGLET TWIST DISTRIBUTION

23

results of the analysis mode were acceptable for verification of the aero-dynamic characteristics of each design.

Figures 10, 11, and 12 illustrate various views of the analysis elements employed within the finite element theory of Reference 9 for one of the wing-winglet configurations. The apparent mismatch in elements along streamwise rows is the result of a limitation of the analysis to planar rectangular analysis elements; however, this mismatch has been shown to be of only minor analytical significance.

An example wing-winglet induced-drag polar predicted by the analysis of Reference 9 is compared in Figure 13 with a polar for the baseline aircraft predicted by the same method. For all wing-winglet configurations, the induced-drag coefficient matched the baseline value at the design lift coefficient of 0.60. For Configuration WW7 (see Figure 13), the entire winglet and baseline drag polars are coincident throughout the lift range. However, typically the winglet drag matched the baseline value only at the design lift coefficient.
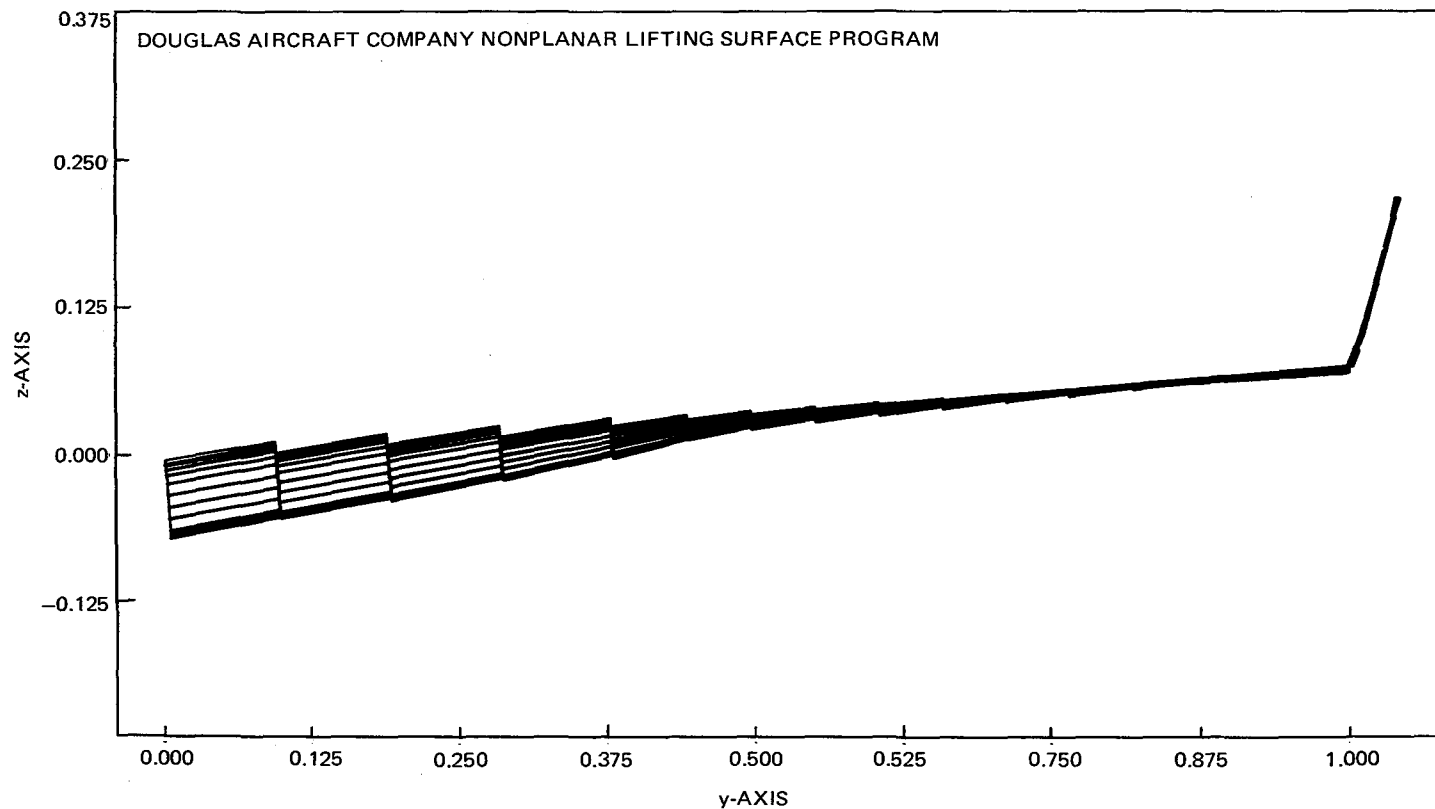
FIGURE 10. AFT VIEW OF LIFTING SURFACE ANALYSIS REPRESENTATION OF WING-WINGLET CONFIGURATION
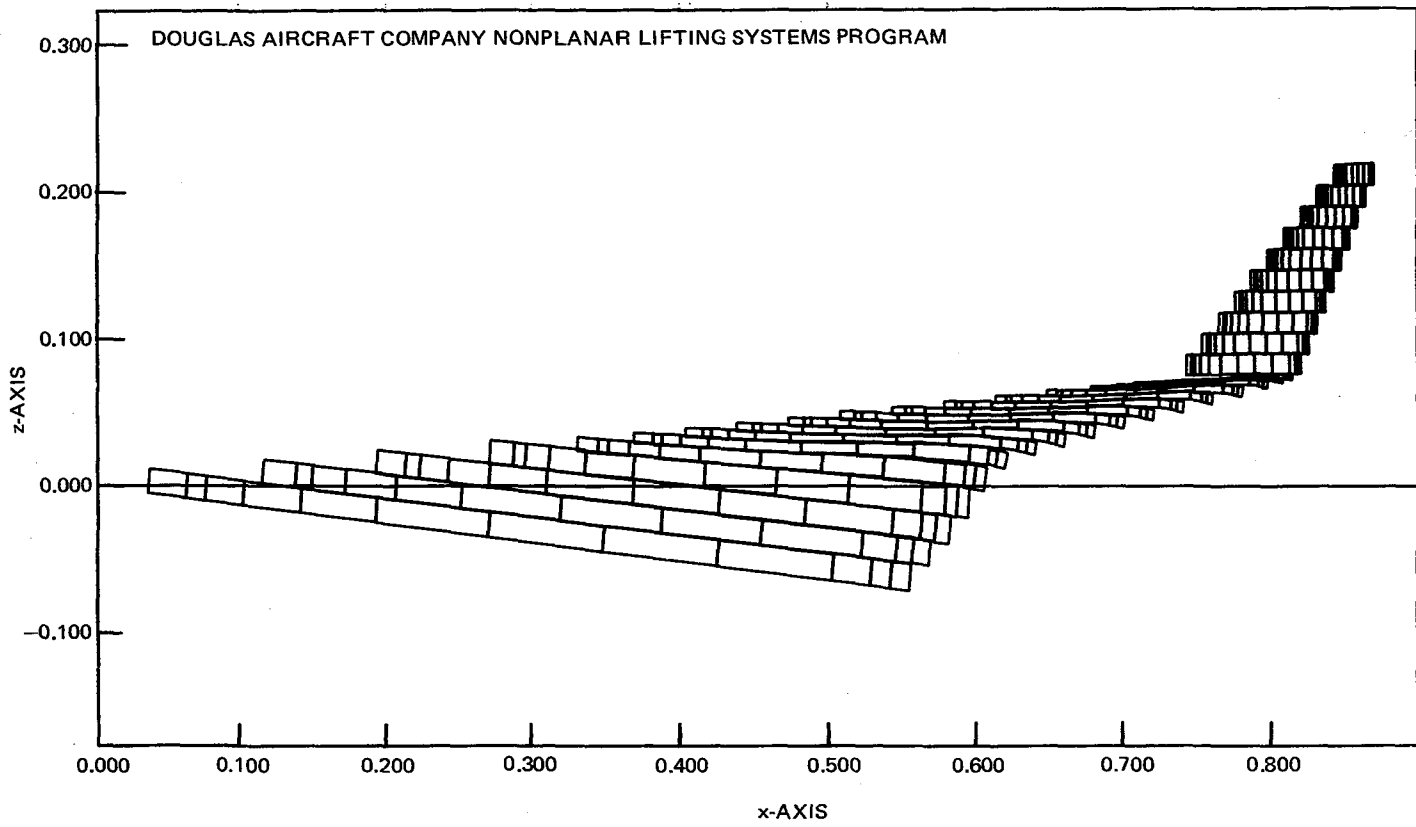
FIGURE 11. SIDE VIEW OF LIFTING SURFACE ANALYSIS REPRESENTATION OF WING-WINGLET
CONFIGURATION
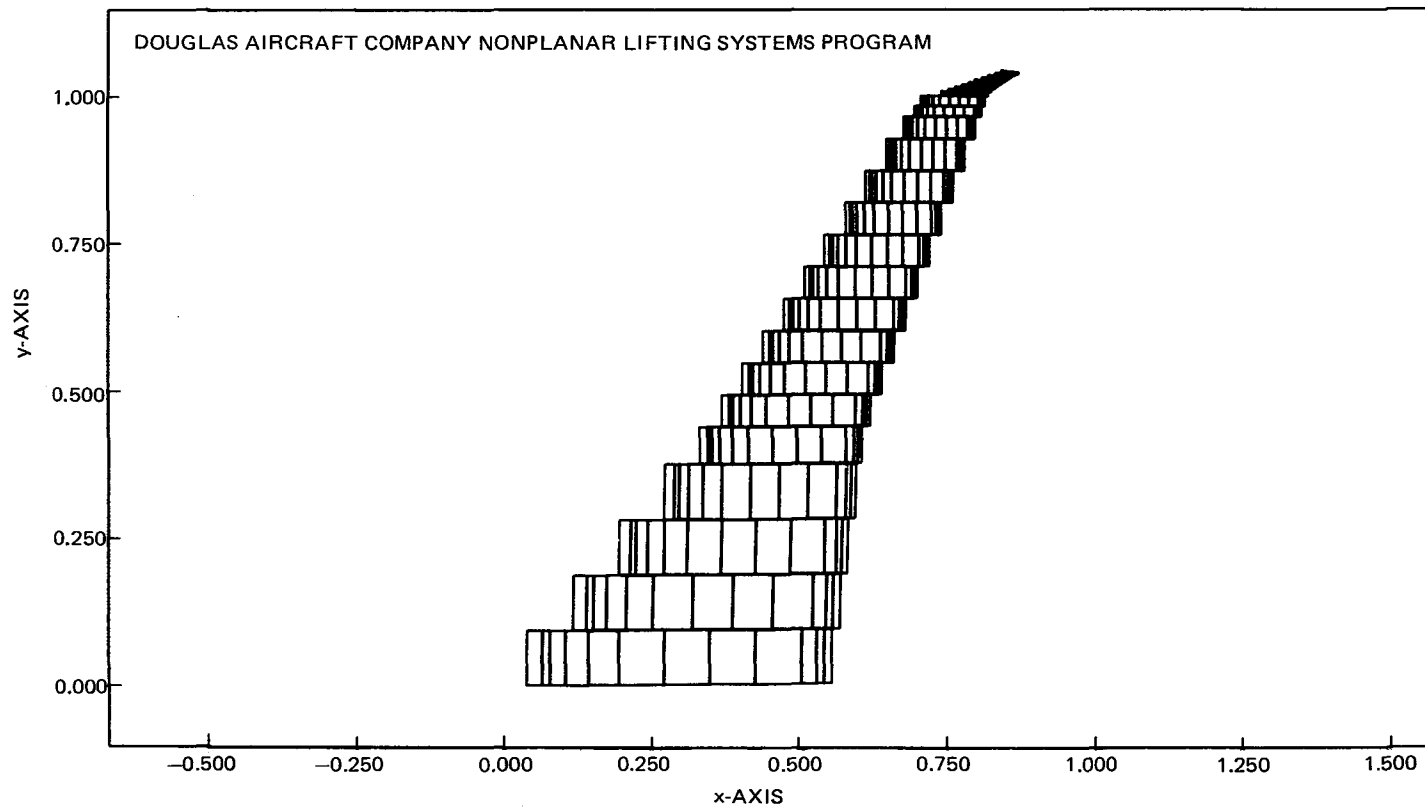
FIGURE 12. PLAN VIEW OF LIFTING SURFACE REPRESENTATION OF WING-WINGLET CONFIGURATION

Aerodynamic Inputs to Structural Analysis. — General aerodynamic loadings
of the wing and winglets were obtained by the method of Reference 8 as pre-
viously described. The aerodynamic loadings of the wing and winglet at
critical design flight conditions were calculated in an iterative manner,
employing initial elastic twist incidences to calculate updated aerodynamic
loads. A second cycle of aerodynamic loading calculations based on updated
elastic twist angles was obtained. These results indicated in general that
a third cycle was unnecessary.
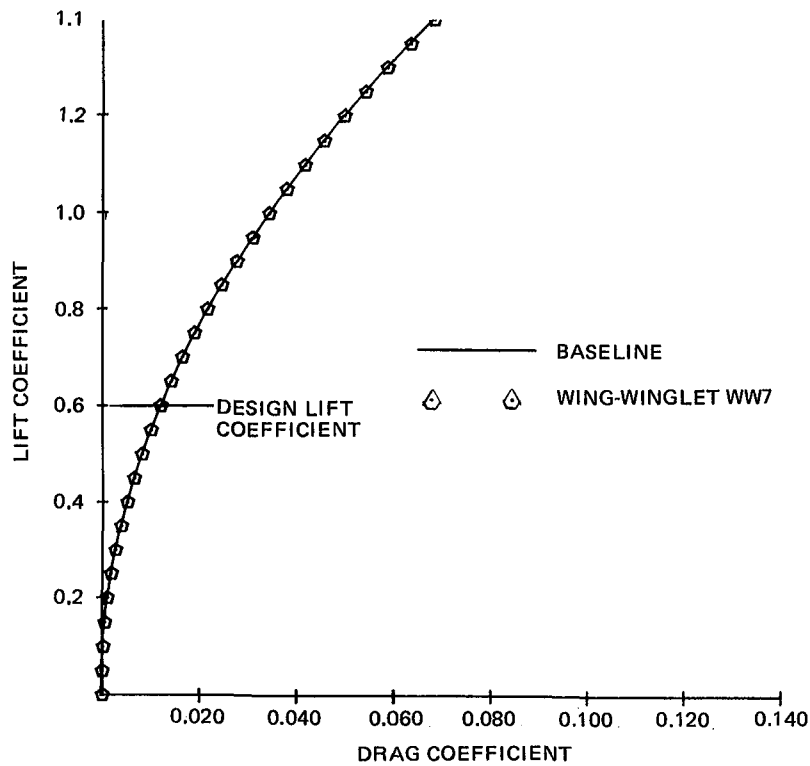
FIGURE 13. COMPARISON OF BASELINE AND WING-WINGLET INDUCED DRAG

Structural Analysis

To determine the structural characteristics of the wing-winglet configuration, both ultimate and flutter modes were considered. Each wing-winglet configuration structure was initially sized for the ultimate mode requirements from which the associated rigidities were derived for flutter evaluation. The structural sizing was then adjusted as necessary to meet the predicted flutter requirements. Analyses described in this section supported both the configuration definition and final configuration evaluation phases.

Strength Analysis. — All configurations, including the conventional baseline design, were subjected to the criteria of FAR Part 25 (Reference 10). Critical maneuver and gust conditions were investigated. The winglet and tip portions of the wing for winglet configurations were determined to be lateral-gust-critical and the wing maneuver-critical. The maneuver and gust conditions selected as critical (from 12 candidate conditions examined) are given in Table 4. All gross weights in the table reflect the fuel expenditure needed to reach the relevant altitude. The total wing load includes horizontal tail and winglet effects. The conditions of Table 4 were applied to all configurations.

In addition to the aeroelastic section twist angles the structural analysis predicted section shear, moment, and torque loads which also included the relieving effect of estimated structural and fuel weight. The wing sections at selected representative stations were then sized for the predicted loads and this resulted in the specification of wing rigidities and inertias. A typical final load calculation is given in Table 5 for wing-winglet configuration WW7 at critical maneuver condition 2. The wing-winglet structure was sized and the resultant rigidity of each configuration was evaluated. Table 6

Table 4

STRUCTURAL DESIGN CONDITIONS

CONDITION NO.	2	12	5
TYPE	Maneuver	Maneuver	Lateral Gust
Gross Weight, kg (lb)	136,303 (300,500)	138,866 (306,150)	125,191 (276,000)
Altitude, m (ft)	7,437 (24,400)	1,524 (5,000)	10,973 (36,000)
Load Factor, N_A	2.5	2.5	1.0
Mach No., M	0.840	0.560	0.800
Velocity, km/hr (keas)	634.9 (342.8)	625.8 (337.9)	463.0 (250.0)
Horizontal Tail Load, kg (lb)	14,061 (-31,000)	3,254 (7,770)	6,804 (-15,000)
Total Wing Load, kg (lb)	354,824 (782,260)	343,643 (757,610)	131,994 (291,000)
Gust Velocity, U_{de}, m/sec (ft/sec)	-	-	15 (50)
Flap Deflection, δ_F (deg)	0	0	0
Spoiler Deflection, δ_{SP} (deg)	0	30	0

Table 5

WINGLET WW7 WING DISTRIBUTED LOADS
(SI UNITS)

NET LOAD DISTRIBUTIONS IN ELASTIC AXIS SYSTEM

SECTION LIFT COEFFICIENT	VERTICAL SHEAR (kN)	HORIZONTAL SHEAR (kN)	LATERAL SHEAR (kN)	STATION (m)	VERTICAL MOMENT (kN·m)	HORIZONTAL MOMENT (kN·m)	TORQUE (kN·m)
0.5114	1	-0.1	-236	0	7179208	1638927	-9857
0.6251	294	-0.1	-237	2.995	7617491	1640263	-10028
0.6253	791	5	-232	3.000	7614499	1620263	-4587282
0.6255	791	5	-232	3.005	7610453	1619923	-4586049
0.6257	805	81	-156	3.010	8890565	1293123	-880712
0.6590	778	79	-140	3.810	8169495	1223717	-850270
0.7177	722	74	-131	5.080	7082798	1091719	-805126
0.7837	654	69	-121	6.350	6082557	960670	-750875
0.8670	569	64	-111	7.720	5118487	827032	-705379
0.8685	705	62	-108	7.750	4848790	748103	-292918
0.9348	620	60	-104	9.010	3890137	661688	-245250
0.9350	621	63	-103	9.020	3897658	639842	-38472
0.9530	579	62	-102	9.650	3447636	593853	-20071
0.9612	545	59	-97	10.160	3113619	548193	-10461
0.9701	461	54	-88	11.430	2364971	450185	10768
0.9722	383	49	-78	12.700	1737837	358898	23025
0.9715	310	44	-69	13.970	1232941	278957	31017
0.9688	251	39	-62	15.240	812197	209507	36167
0.9653	185	36	-55	16.510	500022	148813	39086
0.9492	127	32	-49	17.780	276321	95493	39385
0.9416	111	31	-47	18.180	222997	79887	38927
0.9225	89	30	-45	18.640	170212	62513	38142
0.9041	73	30	-45	19.050	131648	48207	38298
0.8858	60	29	-44	19.410	103731	35619	37834
0.8630	50	29	-43	19.710	84126	25271	37632
0.8603	42	29	-42	19.960	70504	16757	37392
0.8692	36	29	-42	20.150	61829	10238	37076
0.8614	31	29	-42	20.290	56519	5468	36805
0.8275	28	29	-42	20.380	53692	2718	36672
0.1504	28	29	-42	20.399	52884	1949	36786
0.0753	27	29	-42	20.401	52785	1683	36816
0.0	0	0	0	20.404	0	0	0

Table 5 (Continued)

WINGLET WW7 WING DISTRIBUTED LOADS
(CUSTOMARY UNITS)

NET LOAD DISTRIBUTIONS IN ELASTIC AXIS SYSTEM

SECTION LIFT COEFFICIENT	VERTICAL SHEAR (LB)	HORIZONTAL SHEAR (LB)	LATERAL SHEAR (LB)	STATION (IN.)	VERTICAL MOMENT (IN.-LB)	HORIZONTAL MOMENT (IN.-LB)	TORQUE (IN.-LB)
0.5114	232	-20	-53230	0.0	63541360	14505064	-87238
0.6251	-65978	-20	-53198	117.900	67417392	14516899	-88747
0.6253	177772	1080	-52133	118.100	67390912	14339887	-40599008
0.6255	177716	1080	-52130	118.300	67355104	14336868	-40588096
0.6257	180905	18278	-35030	118.500	78684528	11444575	-7784602
0.6599	174720	17839	-34129	150.000	72302816	10830319	-7525177
0.7177	162275	16726	-31844	200.000	62685184	9662086	-7125819
0.7837	146928	15572	-29473	250.000	53832704	8502255	-6716299
0.8670	127958	14403	-27075	303.900	45300352	7319516	-6242842
0.8685	158394	13865	-26233	304.900	42913440	6621495	-2592428
0.9348	139338	13448	-25369	354.700	34429040	5856167	-2170546
0.9350	139576	14059	-23224	354.900	34495600	5662819	-340486
0.9530	129993	13825	-22798	380.000	30512752	5255799	-177633
0.9612	122370	13256	-21772	400.000	27556592	4851691	-92582
0.9701	103695	12174	-19821	450.000	20930800	3984294	95302
0.9722	86117	10956	-17625	500.000	15380449	3176370	203780
0.9715	69689	9832	-15599	550.000	10823442	2468865	274510
0.9688	54391	8841	-13813	600.000	7188222	1854209	320090
0.9653	40086	8007	-12308	650.000	4425366	1317048	345481
0.9492	27541	7274	-10986	700.000	2445532	845152	348572
0.9416	23955	7063	-10598	715.700	1973598	707025	344514
0.9225	19904	6814	-10165	733.900	1506433	553261	337572
0.9041	16391	6736	-10012	749.900	1165129	426647	338946
0.8858	13579	6599	-9773	764.000	918056	315241	334844
0.8630	11315	6522	-9634	775.900	744547	223655	333059
0.8603	9499	6461	-9527	785.800	623985	148307	330934
0.8692	7979	6443	-9492	793.400	547203	90603	328135
0.8614	6909	6426	-9463	798.900	500211	48994	325732
0.8275	6283	6417	-9447	802.200	475195	24056	324562
0.1504	6190	6415	-9443	803.100	468039	17248	325567
0.0753	6189	6415	-9443	803.200	467164	16493	325834
0.0	0	0	0	803.300	0	0	0

Table 6

WING BOX WEIGHT AND RIGIDITY OF CONFIGURATION WW7

SI UNITS

① η	② y_{cw} m	③ t/c	④ C m	⑤ t m	⑥ M (10^{-6}) m-kg	⑦ Critical Condition	⑧ Fe (10^{-3}) PA	⑨ I m^4	⑩ Ac m^2	⑪ C_s m	⑫ t_{sk} m	⑬ J m^4	⑭ ω kg/m	⑮ X_{EA} m	⑯ ΔX_{EA} m	⑰ ΔW kg/side
0	0	0.1500	11.20	1.37	0.9065	2	317,000	0.0289	0.04240	3.91	0.00650	0.053336	234.7	0		
															3.01	706.2
0.148	3.01	0.1500	9.15	1.37	0.9065	2	317,000	0.0289	0.04240	3.91	0.00650	0.053336	234.7	3.01		
															2.30	539.3
0.249	5.08	0.1415	7.74	1.09	0.7223	2	317,000	0.0183	0.04235	3.02	0.00841	0.033648	234.5	5.31		
															2.95	727.6
0.378	7.72	0.1232	5.93	0.73	0.5219	2	310,000	0.0090	0.04685	2.36	0.01191	0.017186	259.3	8.26		
															2.13	507.1
0.473	9.65	0.1185	5.10	0.60	0.3515	2	303,000	0.0052	0.03900	1.98	0.01181	0.009823	215.9	10.39		
															3.48	607.8
0.622	12.70	0.1185	4.26	0.50	0.1772	2	296,000	0.0022	0.02409	1.60	0.00904	0.004200	133.4	13.87		
															4.34	417.3
0.809	16.51	0.1185	3.21	0.38	0.0517	12	262,000	0.00059	0.01060	1.12	0.00569	0.001030	58.8	18.21		
															2.44	117.0
0.914	18.64	0.1185	2.62	0.31	0.0184	5	179,000	0.00023	0.00674	0.86	0.00467	0.000431	37.3	20.65		
															2.06	58.5
1.000	20.40	0.1185	2.13	0.25	0.0079	5	179,000	0.000082	0.00356	0.70	0.00312	0.000151	19.6	22.71		

3680.9

See Continuation for Explanatory Notes

Table 6 (Continued)

CUSTOMARY UNITS

① n	② IN. y_{cw}	③ t/c	④ IN. C	⑤ IN. t	⑥ IN.-LB M (10^{-6})	⑦ CRITICAL CONDITION	⑧ PSI Fe (10^{-3})	⑨ IN.^{4} I	⑩ IN.^{2} Ac	⑪ IN. C_s	⑫ IN. t_{sk}	⑬ IN.^{4} J	⑭ LB/IN. ω	⑮ IN. X_{EA}	⑯ IN. ΔX_{EA}	⑰ LB/SIDE ΔW
0	0	0.1500	441.1	54.04	78.68	2	46	69,320	65.72	154	0.256	128,140	13.14	0		
															118.5	1557
0.148	118.5	0.1500	360.2	54.04	78.68	2	46	69,320	65.72	154	0.256	128,140	13.14	118.5		
															90.5	1189
0.249	200.0	0.1415	304.6	43.10	62.69	2	46	44,060	65.64	119	0.331	80,840	13.13	209		
															116	1604
0.378	303.9	0.1232	233.6	28.78	45.30	2	45	21,730	72.61	93	0.469	41,290	14.52	325		
															84	1118
0.473	380.0	0.1185	200.9	23.81	30.51	2	44	12,380	60.45	78	0.465	23,600	12.09	409		
															137	1340
0.622	500.0	0.1185	167.8	19.88	15.38	2	43	5,330	37.34	63	0.356	10,090	7.47	546		
															171	920
0.809	650.0	0.1185	126.3	14.97	4.486	12	38	1,330	16.43	44	0.224	2,475	3.29	717		
															96	258
0.914	733.9	0.1185	103.1	12.22	1.593	5	26	564	10.45	34	0.184	1,035	2.09	813		
															81	129
1.000	803.2	0.1185	83.9	9.94	0.6877	5	26	197	5.52	27.5	0.123	362	1.10	894		

8115

①② $n = \dfrac{y_{cw}}{b/2}$; b/2 = 803.266 in.

③④⑤ $t/c = \dfrac{\text{MAXIMUM AIRFOIL THICKNESS}}{\text{AERODYNAMIC CHORD}}$

⑥ M = LIMIT VERTICAL BENDING MOMENT ABOUT ELASTIC AXIS
(WHICH IS LOCATED MIDWAY BETWEEN FRONT AND REAR SPARS)

⑦ SEE TABLE 8 FOR CONDITION DEFINITION

⑧ Fe = EQUIVALENT ALLOWABLE STRESS $\approx 0.90\ Fc_{ult}$
Fc_{ult} = ESTIMATED TYPICAL COMPRESSION ALLOWABLE.
SECONDARY EFFECTS ARE COVERED BY 0.90 FACTOR

⑨ I = BENDING STIFFNESS $= \dfrac{M_{ult}\ h}{Fe} = \dfrac{1.5M\ t}{2\ Fe} = \dfrac{0.75\ ⑥⑤}{⑧}$
M_{ult} = 1.5 M; h = t/2 (SYMMETRICAL SECTION)

⑩ Ac = AREA OF COVER PANEL $= \dfrac{I}{2\ h^2_{ave}} = \dfrac{I}{(2)\ (0.425\ t)^2} = \dfrac{2.768⑨}{⑤^2}$
$h_{ave} \approx 0.85\ h = 0.85\ t/2 = 0.425\ t$

⑪ C_s = BOX STRUCTURAL CHORD (NORMAL TO ELASTIC AXIS)

⑫ $t_{sk} = K\bar{t} = 0.60\ \dfrac{Ac}{C_s} = 0.60\ \dfrac{⑩}{⑪}$
$\bar{t} = \dfrac{Ac}{C_s}$; $K = t_{sk}/\bar{t} \approx 0.60$

⑬ J = TORSIONAL STIFFNESS $= \dfrac{4\ A^2}{\int \dfrac{ds}{t_{sk}}} = \dfrac{4\ (0.85\ t\ c_s)^2\ t_{sk}}{2\ (C_s + 0.85\ t)}$
$= \dfrac{1.445⑤^2\ ⑪^2\ ⑫}{⑪ + 0.85⑤}$
A = ENCLOSED AREA $\approx 0.85\ h\ C_s$; dS = PERIMETER; ASSUME t_{sk} = CONSTANT

⑭ ω = BENDING MATERIAL WEIGHT (#/INCH of ELASTIC AXIS SPAN)
$= 2\ A_c\ \rho = 0.2\ ⑩$

⑮ X_{EA} = ELASTIC AXIS STATIONS

⑯ ΔX_{EA} = SPAN INCREMENTS BETWEEN X_{EA} STATIONS

⑰ $\Delta W = \omega_{ave}\ \Delta X_{EA} = ⑭\ ⑯$

34

summarizes the wing box sizing and rigidity results for the WW7 configuration. Identical procedures were completed for each wing and winglet structure.

Flutter Analysis. — Since the shortest wing-winglet configuration (WW2) was unacceptable from an aerodynamic buffet viewpoint, only the remaining three configurations — WW4, WW5, and WW7 (see Figure 5) — were analyzed for flutter integrity. The flutter analysis idealization represented the fuselage, wing, winglet, and engine pylon flexibility but the empennage was considered to be rigid.

Figure 14 shows the spanwise distributions of wing rigidities for the WW4 wing-winglet configuration as prescribed by the ultimate strength analysis described in the previous section.

Experience has indicated that for configurations such as the DC-10 and present baseline aircraft, the flutter speeds associated with antisymmetric motion are very high and not critical. Therefore, only symmetric flutter modes were analyzed. Unsteady aerodynamic influence coefficients were calculated for symmetric motion at a Mach number of 0.79 by application of the doublet lattice method of Reference 11. This method is a finite-element aerodynamic lifting surface analysis which represents the lifting surface by a network of line-doublet potential-flow singularities and employs a control point on each element to impose inviscid tangential flow conditions. This method employs an inviscid unsteady potential flow theory. All aerodynamic coupling among the fuselage, wing, winglet, nacelle, pylon, and horizontal stabilizer was modeled. The theoretical aerodynamic influence coefficients were weighted to reflect available estimated steady aerodynamic data which were collected from wind tunnel tests of comparable configurations.

The modal representation employed consisted of 3 rigid body modes, 10 flexible wing modes, 5 flexible winglet modes, 1 wing roll mode, 3 flexible pylon modes, and 7 fuselage modes.

With respect to the flutter evaluation, certain qualifications need to be recognized. First, the degree of confidence usually associated with conventional wing flutter analysis was not possible since experimental flutter results for a similar wing-winglet configuration were not available for a
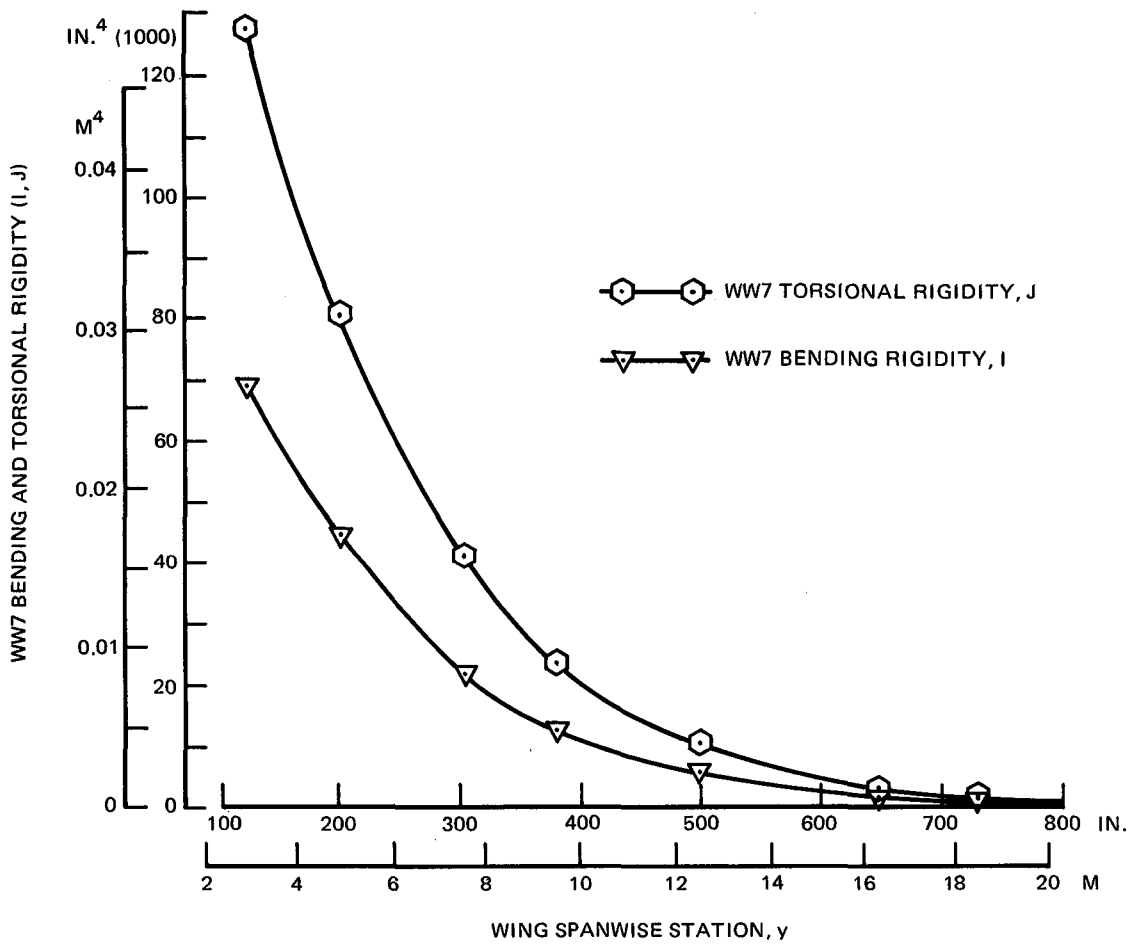
FIGURE 14. WING-WINGLET CONFIGURATION RIGIDITY PROPERTIES

methodology confirmation. Low- and high-speed wind tunnel tests employing elastic flutter models are required to remove this uncertainty. Secondly, the coupling of steady and unsteady aerodynamic effects, which is usually a negligible second order effect on a conventional wing, has been ignored in the present analysis. However this coupling may be as significant for the wing-winglet combination as it is for T-tail configurations. Finally, since all configurations employed advanced supercritical airfoils, their nonlinear compressible characteristics may impact the flutter aerodynamics. In the flutter evaluation, the change of lift curve slope at high subsonic Mach number and low lift coefficient requires futher investigation. The effect pertains to the baseline as well as the wing-winglet configurations, and has not been evaluated for flutter to date.

The flutter analyses were performed for the entire fuel schedule. As shown in the summary of computed flutter speeds (Figure 15), two flutter modes exist for each wing-winglet configuration. The lower-frequency (3.5 Hz) mode is the basic wing inner panel bending/torsion mode which is evident even without the presence of the winglet. For low fuel conditions (less than 20 percent fuel), this flutter mode is of the "mild humping" type (damping decreases gradually as airspeed increases). Note that the WW7 configuration meets the flutter margin requirement (i.e., flutter speed in excess of 1.2 times the dive speed) for this mode, while the other two configurations (WW4 and WW5) do not.

In addition to the 3.5-Hz mode, a higher frequency (4.5-Hz) flutter mode was predicted for each of the wing-winglet configurations. The higher frequency mode was an outer wing torsion mode introduced by the large vertical displacement between the winglet center of mass and the wing plane. As a result, the flutter speed is very sensitive to wing span. The predicted flutter speed for this
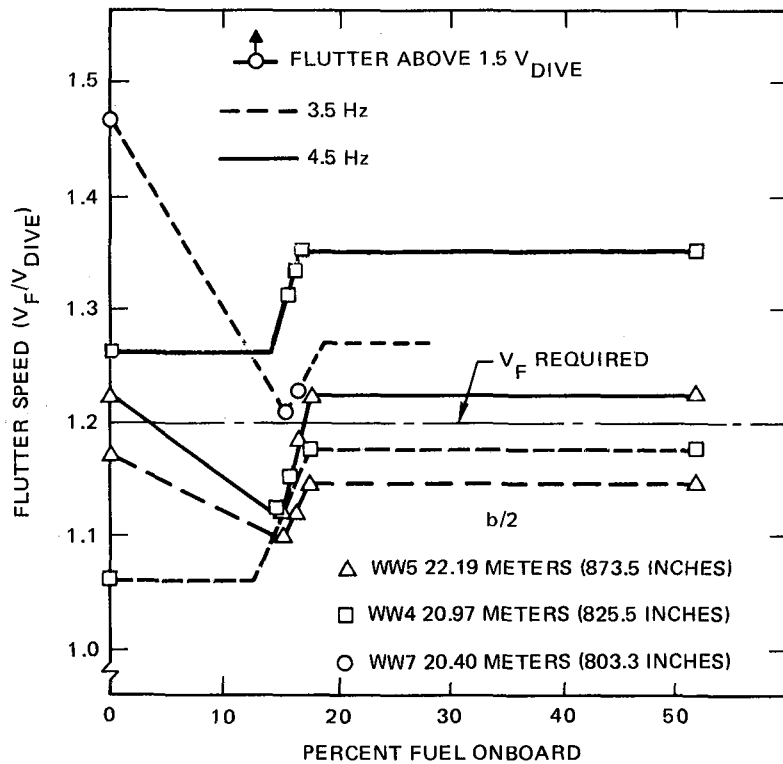
FIGURE 15. WING-WINGLET CONFIGURATION FLUTTER SPEED

mode, as indicated in Figure 15, was below the requirement only for the longest
span configuration (WW5). The other configurations (WW7 and WW4) were acceptable.

An assessment was made of the additional structural weight needed to increase
the flutter speeds of the deficient configurations to the required margin of 20
percent in excess of the dive speed. Analysis of the WW7 configuration indicated
that the ultimate-strength design met the required flutter criteria. Predictions
indicated that the WW4 configuration was deficient in flutter speed margin only
for the wing inner panel bending/torsion 3.5-Hz mode. Analysis showed that
structural stiffening of the inner panel, resulting in a 318-kilogram (700-
pound) weight addition, would increase the flutter speed to the required value.
The distribution of added structure was based on formal optimization analyses
of the baseline aircraft. For the WW5 configuration, the flutter weight penalty
was determined to also be approximately 318 kilograms (700 pounds) to provide

38

sufficient flutter margin for the 3.5-Hz mode. However, the outer wing also required stiffening to meet the flutter speed criteria of the 4.5-Hz mode. The precise amount of the additional stiffening was not determined since it was clearly more than several hundred kilograms and therefore disqualified the WW5 configuration from further contention.

Detailed Weight Evaluation

The weight of the basic wing-winglet lift systems was evaluated for configuration selection and configuration resizing. A weight breakdown of the resized configuration was prepared for input to the direct-operating-costs evaluations. All these estimations employed similar methodology.

Three basic techniques were employed in the weight estimation. First, portions of the aircraft were common with the parent DC-10 aircraft and, consequently, these common components have known weight characteristics which were incorporated into the weight estimates. In the second technique, weights for new major structural components were derived using multistation analysis techniques which consider design criteria, geometry, and loads. The third technique predicted the weights for the remaining new structure and systems by application of parametric relationships isolated during post-design analyses of production aircraft.

During the configuration selection phase of the present study, incremental wing-winglet configuration weights relative to the baseline aircraft were examined since only wing structure changes were of interest. For all config-

urations, the trapezoidal wing area was maintained constant at 202.1 square meters (2175 square feet) to ensure a consistent comparison.

Table 7 presents the basic geometrical characteristics of the baseline aircraft and wing-winglet aircraft, as well as a tabulation of weight increments (relative to the baseline aircraft) of various wing components for the wing-winglet combination. The bending material estimate given in Table 7 was obtained directly from the static structural analysis described earlier which considered gust- and maneuver-load ultimate strength requirements. The weight of additional structure (in excess of static requirements), which was considered to be needed to meet dynamic structural requirements, is listed as a flutter penalty. All other categories given in Table 7 are in addition to these static and dynamic structural requirements.

Table 7

COMPARISON OF BASELINE AND WING-WINGLET CONFIGURATION ESTIMATED WEIGHTS

BASIC WING TRAP	BASELINE WING	WING-WINGLET WW2	WW4	WW5	WW7
Wing Area/Wing Semispan, m²/m (ft²/in.)	202.1/23.41 (2175/921.7)	202.1/19.92 (2175/784.3)	202.1/20.97 (2175/825.5)	202.1/22.19 (2175/873.5)	202.1/20.40 (2175/803.2)
Aspect Ratio	10.85	7.856	8.702	9.745	8.241
Taper Ratio	.1407	.2964	.2490	.1950	.2742
Quarter	30°	30°	30°	30°	30°
WINGLET (ONE SIDE)					
Area/Span m²/m (ft²/in)		3.33/2.95 (35.88/116.1)	2.83/3.10 (32.11/122.2)	2.42/3.28 (26.13/129.3)	3.22/3.02 (34.67/118.7)
Aspect Ratio		2.608	3.23	4.442	2.831
Taper Ratio		.300	.300	.300	.300
TAKEOFF GROSS WEIGHT, kg (lb)	138,798 (306,000)	138,798 (306,000)	138,798 (306,000)	138,798 (306,000)	138,798 (306,000)
FLAPERON	No	No	No	No	No
BENDING MATERIAL	8,100 (17,858)	7,496 (16,526)	7,413 (16,342)	7,731 (17,044)	7,362 (16,230)
BENDING MATERIAL		-604 (-1332)	-688 (-1516)	-369 (-814)	-738 (-1628)
SPAR WEBS		-49 (-107)	-30 (-67)	-13 (-29)	-40 (-88)
RIBS		96 (+211)	64 (+140)	30 (+66)	80 (+177)
WINGLET AND ATTACH		303 (+669)	278 (+612)	262 (+578)	295 (+650)
LEADING EDGE		-93 (-204)	-74 (-164)	-56 (-124)	-69 (-152)
LEADING EDGE FLAPS		-127 (-280)	-104 (-230)	-82 (-180)	-97 (-214)
TRAILING EDGE		131 (+288)	103 (+228)	76 (+168)	92 (+202)
SPOILERS		-67 (-148)	-81 (-178)	-94 (-208)	-76 (-167)
FLAPS		0	0	0	0
AILERON		7 (+16)	5 (+12)	4 (+8)	8 (+18)
TIP		-17 (-38)	-17 (-38)	-17 (-38)	-17 (-38)
SUB-TOTAL		-420 (-925)	-545 (-1201)	-260 (-573)	-562 (-1240)
FLUTTER PENALTY		>318 (+>700)	318 (+700)	>318 (+>700)	0
TOTAL INCREMENTAL WEIGHT		-102 (-225)	-227 (-501)	58 (+127)	-562 (-1240)
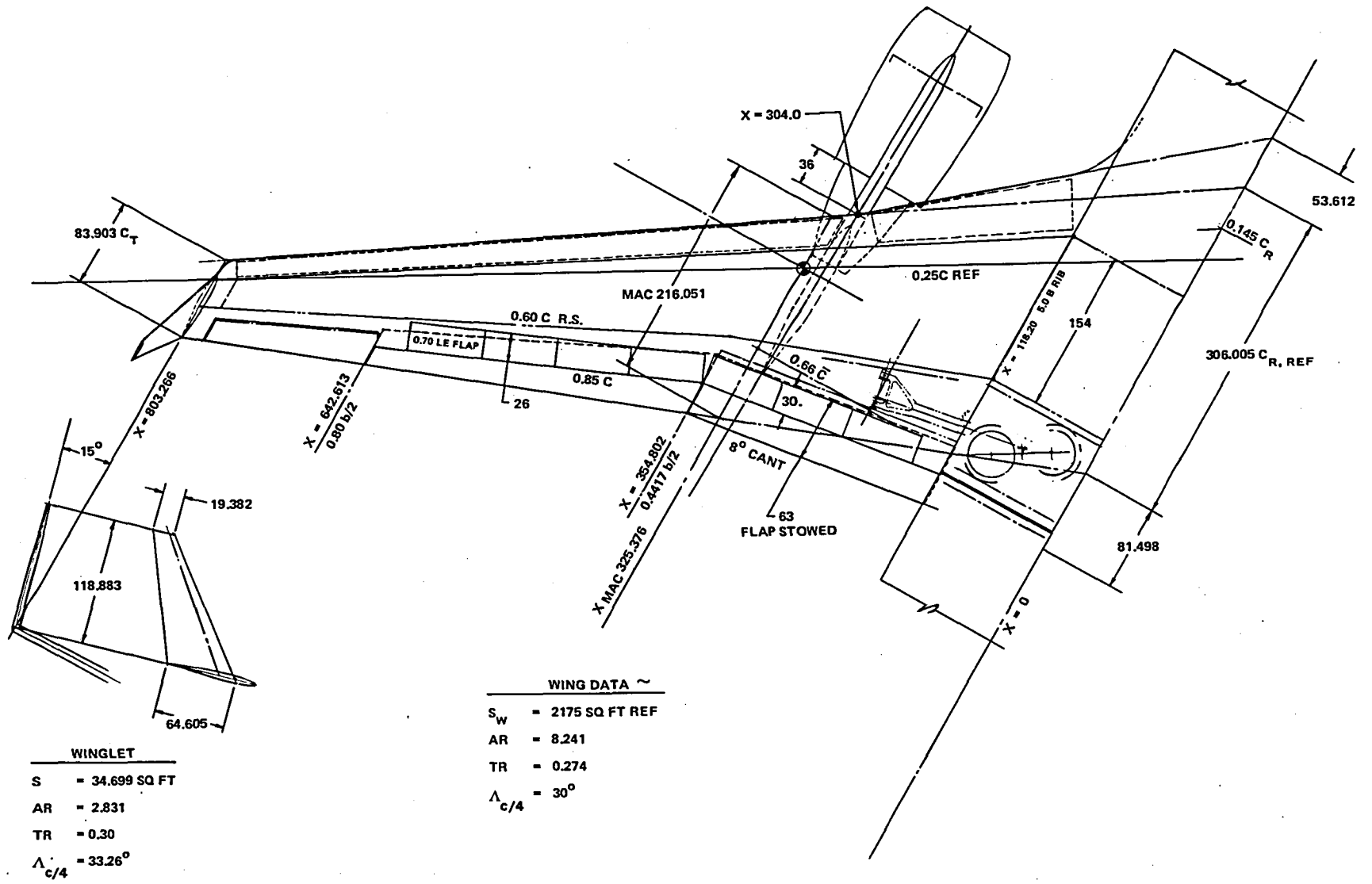
FIGURE 16. STRUCTURAL LAYOUT OF FINAL WING-WINGLET CONFIGURATION

42

Configuration Selection

The combination of the aerodynamic design, structural analysis and weight
estimation results in four wing-winglet configurations of nearly equivalent
aerodynamic capabilities but varying structure and weight characteristics.
Table 8 compares each wing-winglet configuration with the baseline aircraft
employing a conventional wing. At the left side of the table, the aerodynamic
induced-drag efficiency factor and geometrical characteristics are tabulated.
The right half of the table gives the weights. Although wing bending material
weight is significant for the wing-winglet designs, the weight associated with
meeting the flutter requirement is a nearly dominant factor in determining the
total configuration weight increment relative to the baseline wing.

The relative weight results described above are shown in Figure 17. The
three components of incremental configuration weight of Table 8 are given in
Figure 17, including: wing bending material incremental weight; bending mater-
ial with winglet and miscellaneous weights such as flaps and slats (total wing-
winglet weight exclusive of flutter penalty); and total weight of the wing-
winglet system. Although all three components appear to have a minimum at the
same design point, it is evident that the slope of the weight curve is increased
significantly by inclusion of flutter-related weight. The shortest span config-
uration which satisfies a simple buffet requirement (WW7) is also the lightest
wing-winglet design. Therefore, this configuration was selected for evaluation
and comparison with the baseline wing.

An aircraft configuration based on combination WW7 is shown in the three-
view drawing of Figure 18. The characteristics shown in this figure are based

Table 8

WING-WINGLET CONFIGURATION CHARACTERISTICS

CONFIGURATION	EFFICIENCY FACTOR, e	WING		WINGLET		CONFIGURATION WEIGHT kg (lb)		CONFIGURATION WEIGHT RELATIVE TO BASELINE kg (lb)		
		SEMISPAN, m (in)	ASPECT RATIO	SPAN, m (in)	ROOT CHORD, m (in)	BENDING MATERIAL	FLUTTER PENALTY	BENDING MATERIAL	BENDING MATERIAL WINGLET AND MISC	TOTAL (INCLUDING FLUTTER REQUIREMENTS)
Baseline	0.90	23.41 (921.7)	10.85	-	-	8,100 (17,858)	0	-	-	-
WW5	0.97	22.19 (873.5)	9.73	3.284 (129.3)	1.15 (45.1)	7,731 (17,044)	>318 (>700)	-369 (-814)	-260 (-573)	>58 (>127)
WW4	1.09	20.97 (825.5)	8.70	3.104 (122.2)	1.48 (58.2)	7,413 (16,342)	318 (700)	-688 (-1516)	-545 (-1201)	-227 (-501)
WW7	1.15	20.40 (803.3)	8.24	3.020 (118.9)	1.64 (64.6)	7,362 (16,230)	0	-738 (-1628)	-562 (-1240)	-562 (-1240)
WW2B	1.21	19.92 (784.3)	7.86	2.949 (116.1)	1.79 (70.4)	7,496 (16,526)	UNKNOWN	-604 (-1332)	-420 (-925)	UNKNOWN

44
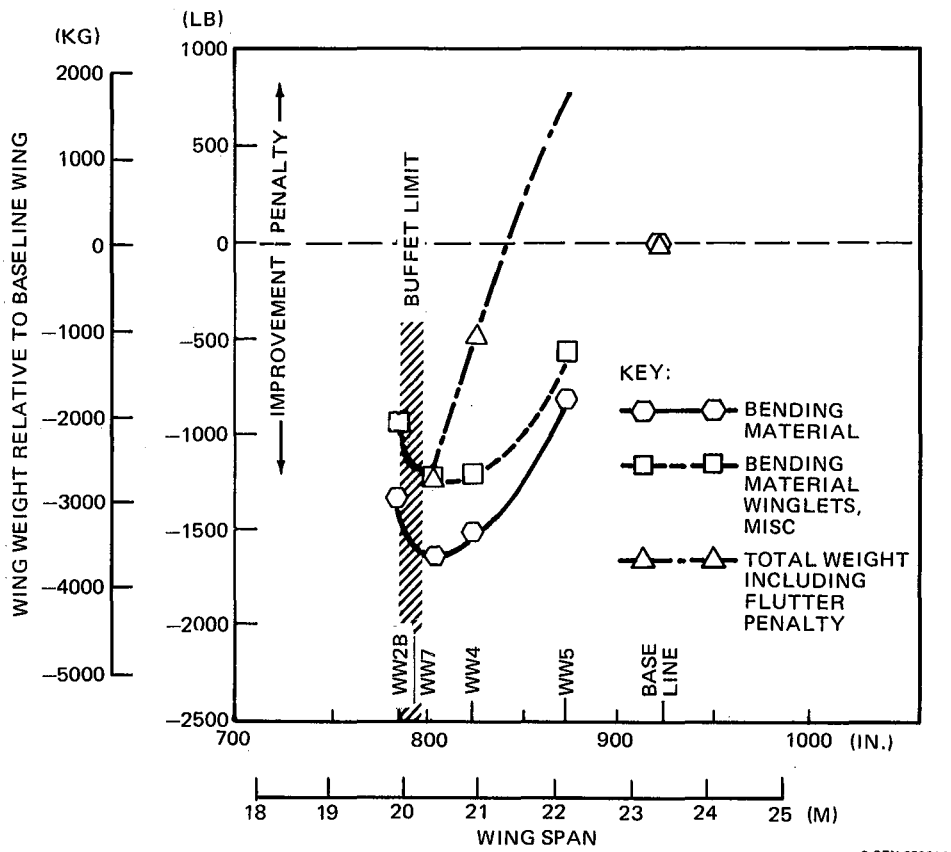
FIGURE 17. CONFIGURATION WEIGHT INCREMENTS

on the preliminary size aircraft (e.g., 202.1-square meter, or 2175-square foot, wing trapezoidal area) and do not reflect the final sizing of the aircraft.

CHARACTERISTICS DATA			
⊙ ITEM	WING	HORIZONTAL TAIL	VERTICAL TAIL
AREA, SQ m (SQ FT)	202.1 (2175)	56.7 (610)	37.6 (405)
ASPECT RATIO	8.24	3.8	1.6
TAPER RATIO	0.27	0.35	0.35
SWEEP, c/4	30°	30°	35°
DIHEDRAL, c/4	4°	10°	—

41.96 m
(137 FT 8 IN.)

43.43 m
(142 FT 6 IN.)

15.21 m
(50 FT)
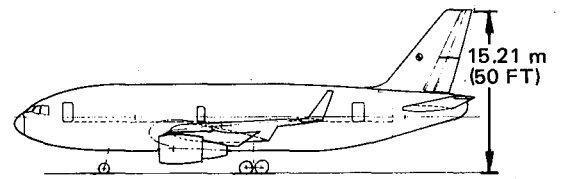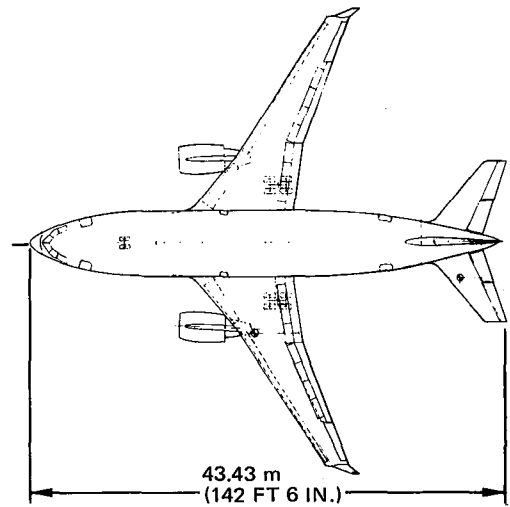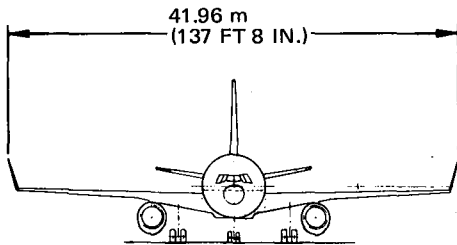
8-GEN-25884

FIGURE 18. SELECTED WING-WINGLET CONFIGURATION

46

At the conclusion of the configuration selection phase of the study, a basic wing-winglet combination was available for comparison with a conventionally designed wing. Detailed aerodynamic characteristics were first estimated to facilitate sizing-performance calculations. The aircraft were then resized and performance was estimated for a typical mission. Direct operating costs were then estimated and evaluated.

Estimation of Aerodynamic Characteristics of Final Wing-Winglet Configuration

For the preliminary configuration selection phases, only load distribution and lift-induced drag were of significance. In the detailed evaluation, cruise and high-lift aerodynamic characteristics were estimated (using conventional methods) in conjunction with the lifting surface numerical analysis method of Reference 9. In addition, the estimates of previously determined characteristics were refined.

Cruise-drag characteristics were estimated by summing parasite, induced, compressibility, and trim drag contributions:

$$C_{D_{total}} = C_{D_{parasite}} + C_{D_{induced}} + \Delta C_{D_{compressibility}} + \Delta C_{D_{trim}}.$$

Parasite drag, consisting of skin friction, form, and roughness drag, was estimated by applying Clutter skin friction coefficient tables (Reference 12), accounting for the configuration geometry and local Reynolds number. The

cruise-induced drag was based on application of the analysis of Reference 9 and the results are shown in Figure 13. The wing-winglet configuration was designed to match the baseline-induced drag at the design lift coefficient ($C_L = 0.60$). However, the induced drag differed slightly from the baseline values at off-design lift coefficients. Tail-off compressibility drag was assumed to be identical to that of the baseline aircraft. However, a reduction in wing-winglet tail compressibility drag, relative to the baseline value, was estimated as a result of the smaller wing-winglet tail size. The trim drag was calculated by employing moments and downwash at the horizontal tail which were estimated by lifting surface theory analysis of the wing-winglet configuration. Table 9 provides estimated drag components for both the baseline and final wing-winglet configuration at the trimmed lift condition as well as the associated incremental values.

Table 9

DRAG COMPONENT ESTIMATES FOR THE BASELINE
AND WING-WINGLET AIRCRAFT

	$C_{D_{parasite\ \&\ interference}}$	$C_{D_{induced}}$	$\Delta C_{D_{compressibility}}$	$\Delta C_{D_{trim}}$	$C_{D_{total}}$
Baseline	0.0185	0.0112	0.0022	0.0013	0.0332
Wing-Winglet	0.0182	0.0112	0.0022	0.0011	0.0327
Increment, Wing-Winglet-Baseline	-0.0003	+0.0	0.0	-0.0001	-0.0004

Above values are at aircraft lift coefficient of 0.55 which is the approximate trimmed cruise lift coefficient.

Above values are based on wing reference value of 202.1 square meters (2175 square feet).

As in the case of the baseline aircraft, high-lift characteristics were generated for the wing-winglet configuration by employing conventional methods (modified version of Reference 13) in conjunction with predictions based on results of the numerical lifting surface analysis of Reference 9. For example, the aircraft maximum lift coefficient was estimated by adjusting the basic wing maximum lift value by increments resulting from the variable-camber Krueger, trailing-edge flap system, trim lift penalty, and dynamic contributions:

$$C_{L_{max_{V_{min}}}} = C_{L_{max_{basic}}} + \Delta C_{L_{max_{VCK}}} + \Delta C_{L_{max_{flap}}} + \Delta C_{L_{trim}} + \Delta C_{L_{V_{min}}} \ .$$

Basic wing maximum lift capability was assumed to be the same as for the baseline aircraft even though analysis indicated the possibility that the winglet airfoils may require additional sectional maximum-lift capability at the root. Presumably this additional capability could be provided by a winglet root leading edge extension. The impact of the additional maximum lift capability requirement was expected to be minimal and was neglected. The $C_{L_{max_{V_{min}}}}$ and lift-to-drag ratios predicted for the wing-winglet and baseline aircraft are presented in Figures 19 and 20, respectively.

The lower-than-baseline maximum lift values of the wing-winglet combination, evident in Figure 19, resulted from the smaller flapped wing area of the lower-aspect-ratio wing-winglet planform. Slightly degraded wing-winglet lift-to-drag ratios of Figure 20 were estimated based on the inability of the winglet to reduce the induced drag of the flap-dominated configuration as effectively as for the cruise configuration. The "bend" in the landing lift-to-drag ratio curves, which is apparent in Figure 20, resulted from the requirement for additional deflection of the flaps at lift coefficients above the maximum value obtainable with the initial flap deflection (20°/10°).
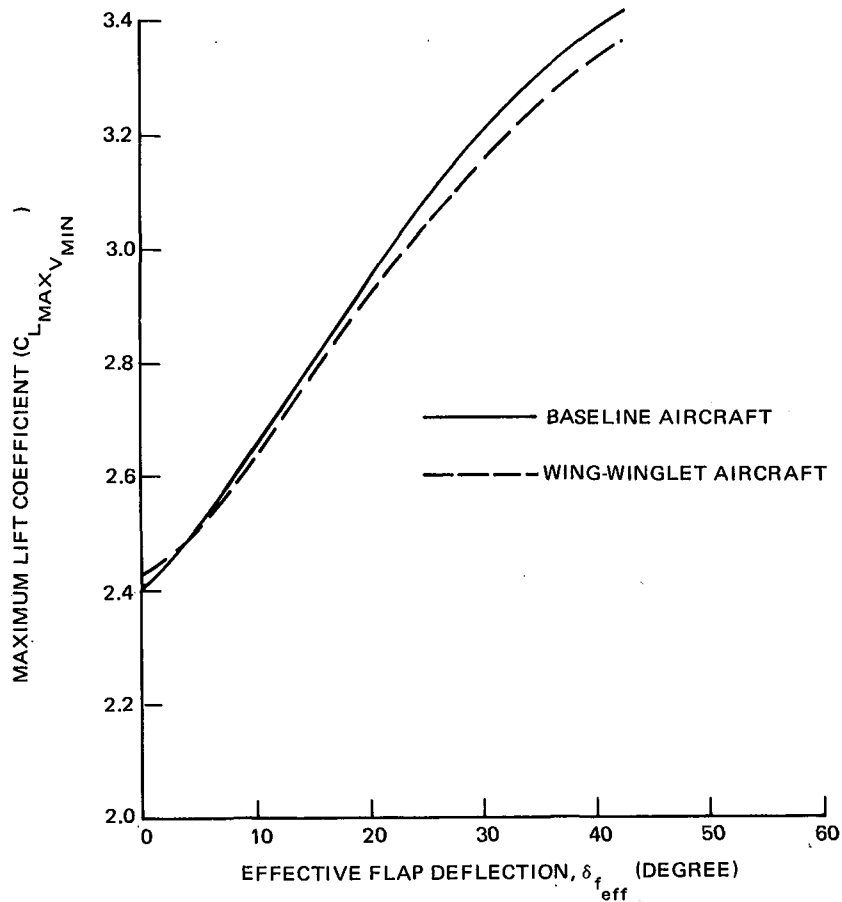
FIGURE 19. ESTIMATED MAXIMUM LIFT COEFFICIENT OF BASELINE AND WING-WINGLET AIRCRAFT

The flap maximum-lift increments for both the baseline and wing-winglet aircraft were estimated by employing unpublished Douglas Aircraft Company two-dimensional experimental data for the proposed two-segment flap. Conversion of the two-dimensional values to three-dimensional maximum-lift increments was performed via a two-dimensional to three-dimensional analogy based on flap system areas and chords.

Low-speed drag was estimated by augmenting the baseline aircraft drag polars with increments (relative to the baseline) for the basic wing-winglet (parasite and induced) drag and the flap induced drag. This approach permitted the use of the baseline aircraft flap parasite drag estimates. Incremental values predicted using the method of Reference 8 were also employed to generate lift curves
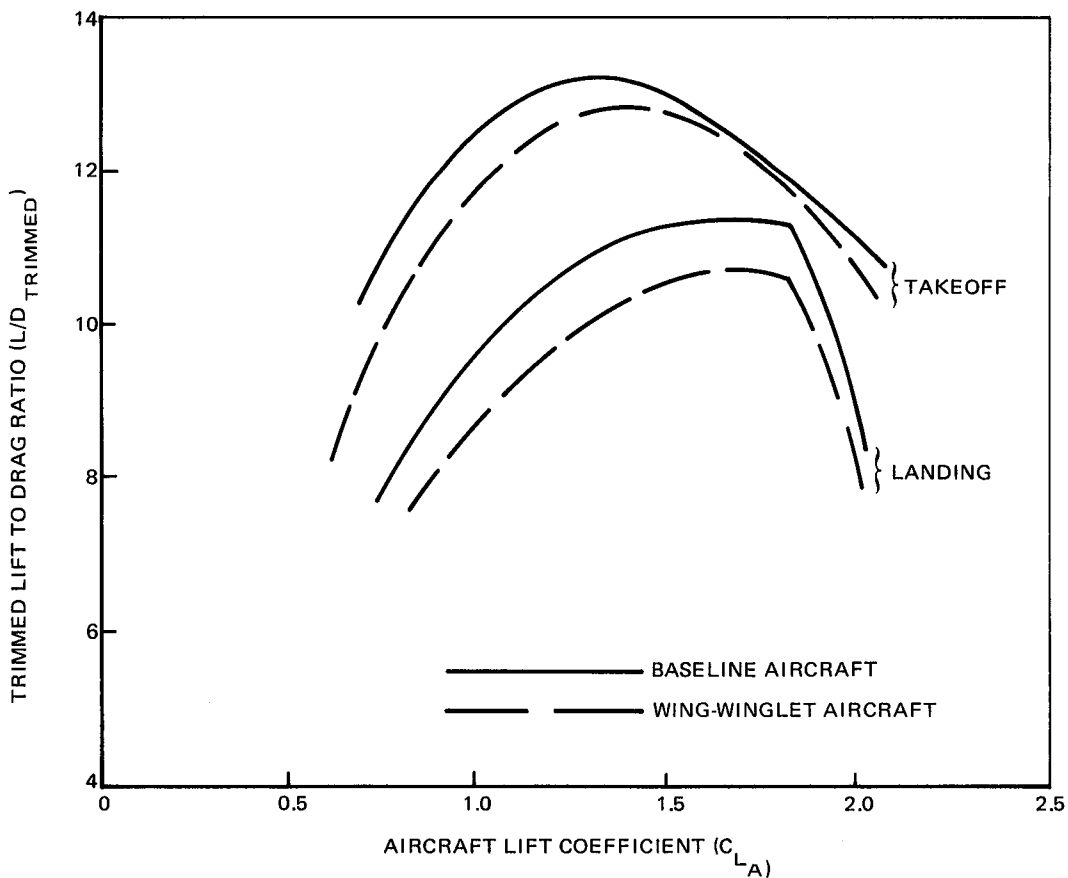
FIGURE 20. ESTIMATED TRIMMED LIFT-TO-DRAG RATIO OF BASELINE AND WING-WINGLET AIRCRAFT

and pitching moments for estimation of lift coefficient at minimum unstick speed $(C_{L_{V_{mu}}})$ and trimmed lift. Figures 21 and 22 give the predicted high-lift system increments in high-lift-system induced drag, flap lift, and pitching moment. The estimated high-lift characteristics of the wing-winglet configuration indicate only a small degradation compared to the characteristics of the higher-aspect-ratio baseline design.

Estimation of Weight Characteristics of the
Selected Wing-Winglet Configuration

Subsequent to the selection of the final wing-winglet configuration, a detailed weight evaluation was performed for the final configuration based on the wing structural drawing of Figure 16. The product of this detailed weight evaluation was a set of weight equations which were input directly to configuration sizing/performance numerical analysis.

The final weight estimation function entailed the calculation of a weight breakdown for the various components of the resized baseline and wing-winglet aircraft. Tables 10 and 11 present the weight breakdown for the baseline and final wing-winglet aircraft. The tables include definition of new and common weight for cost estimating purposes. Components of "common weight" are in current DC-10 production.

Table 10

WEIGHT BREAKDOWN OF RESIZED BASELINE AIRCRAFT

All Weights in Kilograms (Pounds)

Max. Takeoff Weight	133,809 (295,000)				
Max. Landing Weight	117,933 (260,000)				
Max. Zero Fuel Weight	108,862 (240,000)				
Max. Fuel Capacity @ 802.8 kg/m^3 (6.7 lb/gal)	39,462 (87,000)				
Basic Wing Area, m^2 (ft^2)	208 (2,240)				
Horizontal Area - gross/exposed, m^2 (ft^2)	64/53 (684)(572)				
Vertical Area - exposed, m^2 (ft^2)	38 (405)				
Tail Arm Horiz/Vert, m (in)	18.5/17.6 (728.5/691.5)				
Engines	2/CF6-45				
Thrust/Engine, kN (lb)	200.16 (45,000)				

	Total	Common	(1) Gage	New	(2) Estimated DC-10 Cost Commonality (%)
Wing	15,943 (35,148)			15,943 (35,148)	0
Horizontal	1,447 (3,190)			1,447 (3,190)	0
Vertical	1,243 (2,740)			1,243 (2,740)	0
Fuselage	15,676 (34,560)	6,210 (13,690)	2,889 (6,370)	6,577 (14,500)	52.5
Gear (less rolling assembly)	3,683 (8,120)	492 (1,084)		3,191 (7,036)	13.3
Sub-Total	37,992 (83,758)	6,701 (14,774)	2,889 (6,370)	28,401 (62,614)	23.0
Propulsion (less engines)	3,928 (8,660)	2,948 (6,500)		980 (2,160)	75.1
Fuel System	599 (1,320)	118 (260)		481 (1,060)	19.7
Sub-Total	4,527 (9,980)	3,066 (6,760)	0	1,461 (3,220)	67.7

Table 10 (Continued)

Flight Controls	2,173 (4,790)	200 (440)		1,973 (4,350)	9.2
Hydraulics	1,000 (2,205)	458 (1,010)	227 (500)	315 (695)	61.7
APU	562 (1,240)	73 (160)		490 (1,080)	12.9
Instruments	582 (1,284)	341 (751)		242 (533)	58.5
Air-Conditioning	925 (2,040)	812 (1,790)		113 (250)	87.7
Pneumatics	579 (1,276)	337 (743)		242 (533)	58.2
Electrical	1,352 (2,980)	1,005 (2,215)		347 (765)	74.3
Lighting	662 (1,460)	576 (1,270)		86 (190)	87.0
Avionics	686 (1,512)	586 (1,291)		100 (221)	85.0
Furnishings					
Fixed	6,808 (15,010)	5,480 (12,081	421 (928)	908 (2,001)	84.8
Seats	3,456 (7,620)	3,456 (7,620)			100.0
Galleys	1,449 (3,195)	1,449 (3,195)			100.0
Anti-Ice	172 (380)	92 (203)		80 (177)	53.4
Aux. Gear	23 (50)		23 (50)		70.0
Sub-Total	20,431 (45,042)	14,864 (32,769)	670 (1,478)	4,896 (10,795)	75.1
Cost Weight	62,949 (138,780)	24,631 (54,303)	3,560 (7,848)	34,758 (76,629)	43.09
Engines	7,960 (17,550)	7,960 (17,550)			100.0
Rolling Assembly	2,354 (5,190)	159 (350)		2,195 (4,840)	6.7
Manufacturer's Empty Weight	73,264 (161,520)	32,750 (72,203)	3,560 (7,848)	36,953 (81,469)	48.10
Op. Items + Weight Allow.	5,974 (13,170)				
Operating Empty Weight	79,237 (174,690)				

(1) Gage weight is assumed to be 30% new and 70% common.
(2) Estimated cost commonality = common + 70% gage.

Table 11

WEIGHT BREAKDOWN FOR FINAL RESIZED WING-WINGLET CONFIGURATION

All Weights in Kilograms (Pounds)

Max. Takeoff Weight	132,448 (292,000)				
Max. Landing Weight	117,479 (259,000)				
Max. Zero Fuel Weight	112,490 (248,000)				
Max. Fuel Capacity @ 802.8 kg/m^3 (6.7 lb/gal)	41,186 (90,800)				
Basic Wing Area, m^2 (ft^2)	209 (2,255)				
Horizontal Area - gross/exposed m^2 (ft^2)	61/51 (657 / 548)				
Vertical Area - exposed, m^2 (ft^2)	38 (405)				
Tail-Arm Horiz/Vert, m (in)	18.6/17.7 (734.3/697.3)				
Engines	2/CF6-45				
Thrust/Engine, kN (lb)	200.16 (45,000)				

	Total	Common	(1) Gage	New	(2) Estimated DC-10 Cost Commonality (%)
Wing	15,435 (34,028)			15,435 (34,028)	0
Horizontal	1,397 (3,080)			1,397 (3,080)	0
Vertical	1,238 (2,730)			1,238 (2,730)	0
Fuselage	15,667 (34,540)	6,205 (13,680)	2,885 (6,360)	6,577 (14,500)	52.5
Gear (less rolling assembly)	3,647 (8,040)	492 (1,084)		3,155 (6,956)	18.5
Sub-Total	37,384 (82,418)	6,697 (14,764)	2,885 (6,360)	27,802 (61,294)	23.3
Propulsion (less engines)	3,928 (8,660)	2,948 (6,500)		980 (2,160)	75.1
Fuel System	601 (1,325)	118 (260)		483 (1,065)	19.6
Sub-Total	4,529 (9,985)	3,066 (6,760)	0	1,463 (3,225)	67.7

Table 11 (Continued)

Flight Controls	2,159 (4,760)	200 (440)		1,960 (4,320)	9.2
Hydraulics	998 (2,200)	458 (1,010)	227 (500)	313 (690)	61.8
APU	562 (1,240)	73 (160)		490 (1,080)	12.9
Instruments	582 (1,284)	341 (751)		242 (533)	58.5
Air Conditioning	925 (2,040)	812 (1,790)		113 (250)	87.7
Pneumatics	579 (1,276)	337 (743)		242 (533)	58.2
Electrical	1,352 (2,980)	1,005 (2,215)		347 (765)	74.3
Lighting	662 (1,460)	576 (1,270)		86 (190)	87.0
Avionics	686 (1,512)	586 (1,291)		100 (221)	85.0
Furnishings					
Fixed	6,808 (15,010)	5,480 (12,081)	421 (928)	908 (2,001)	84.8
Seats	3,456 (7,620)	3,456 (7,620)			100.0
Galleys	1,449 (3,195)	1,449 (3,195)			100.0
Anti-Ice	172 (380)	92 (203)		80 (177)	53.4
Aux. Gear	23 (50)		23 (50)		70.0
Sub-Total	20,415 (45,007)	14,864 (32,769)	670 (1,478)	4,881 (10,760)	75.1
Cost Weight	62,328 (137,410)	24,627 (54,293)	3,555 (7,838)	34,146 (75,279)	43.50
Engines	7,960 (17,550)	7,960 (17,550)			100.0
Rolling Assembly	2,331 (5,140)	145 (350)		2,173 (4,790)	6.8
Manufacturer's Empty Weight	72,620 (160,100)	32,746 (72,193)	3,555 (7,838)	36,318 (80,069)	48.52
Op. Items + Weight Allow.	5,974 (13,170)				
Operating Empty Weight	78,593 (173,270)				

(1) Gage weight is assumed to be 30% new and 70% common.

(2) Estimated cost commonality = common + 70% gage.

Sizing Study

In the configuration selection phase, a trapezoidal wing area of 202.1 square meters (2175 square feet) was employed to enable a consistent comparison of competing wing-winglet designs with varying wing aspect ratios. Prior to the sizing study, an evaluation was made of the design status of the baseline aircraft. From this evaluation it was determined that small changes should be made to the baseline aerodynamic characteristics to ensure consistent comparison with the wing-winglet aircraft.

SQUARE OF TAIL-OFF LIFT COEFFICIENT ($C_{L_{TO}}^2$)

6.0

5.0

4.0

3.0

2.0

1.0

0

0   0.005   0.010   0.015   0.020   0.025

$\Delta\Delta C_{D_i}$

FLAP SETTING

5/10

10/10

15/10

20/10

25/10

35/10

DIFFERENCE BETWEEN WING-WINGLET AND BASELINE AIRCRAFT INCREMENTAL
FLAP DRAG COEFFICIENT, $\Delta C_{D_i}\text{WINGLET} - \Delta C_{D_i}\text{BASELINE}$
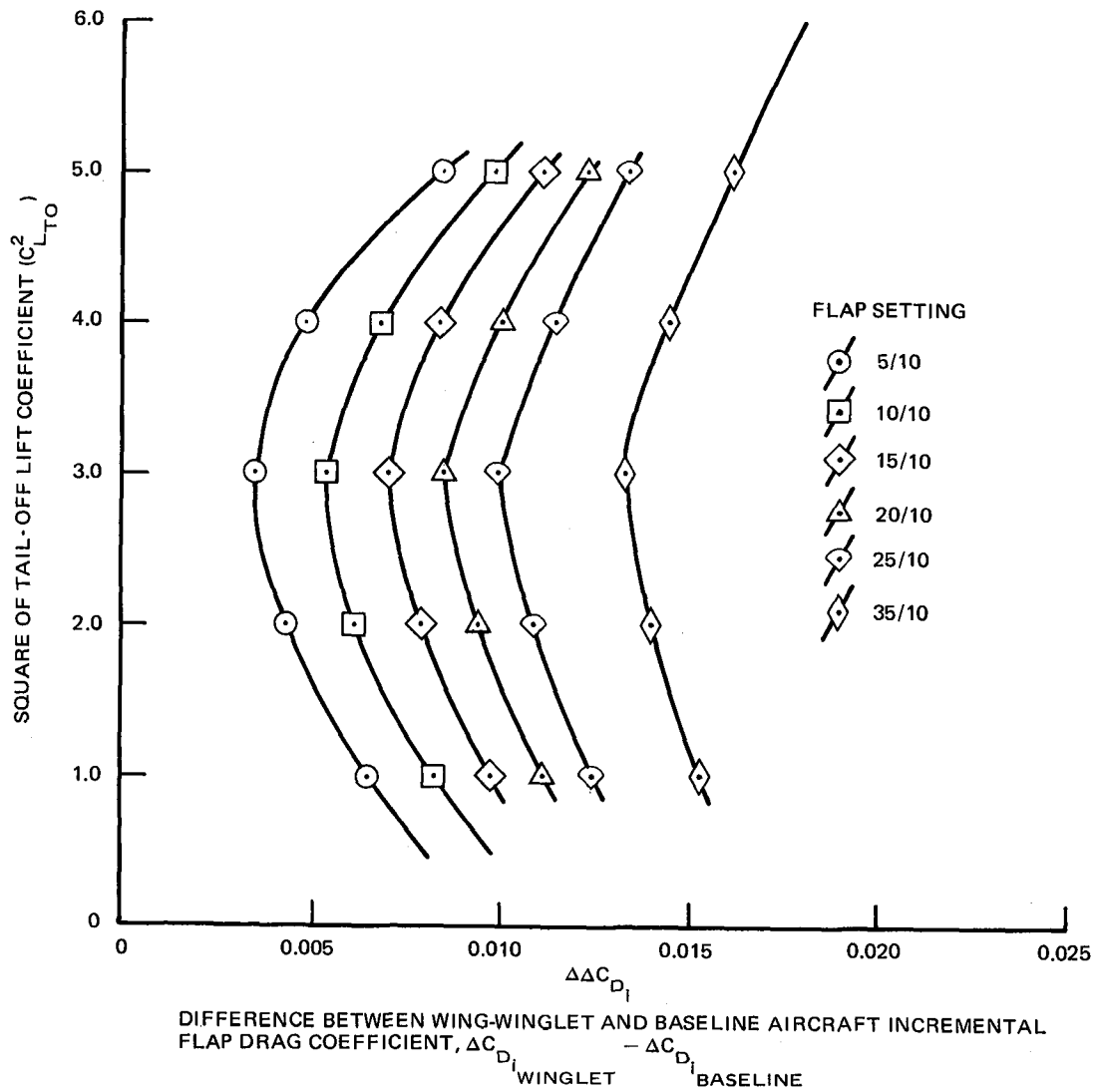
FIGURE 21. ESTIMATED WING-WINGLET AIRCRAFT LOW-SPEED INDUCED DRAG

Accordingly, both the baseline and chosen wing-winglet aircraft were
resized to determine the wing area and minimum takeoff gross weight needed to
meet the design requirements of Table 1.

The sizing process was accomplished by utilizing the sizing feature of a
combined sizing/performance computer analysis. This computer program,
designed specifically for parametric aircraft sizing studies at the
preliminary design level, employs classical equations of motion.
Starting with an initial estimate for takeoff gross weight, the program
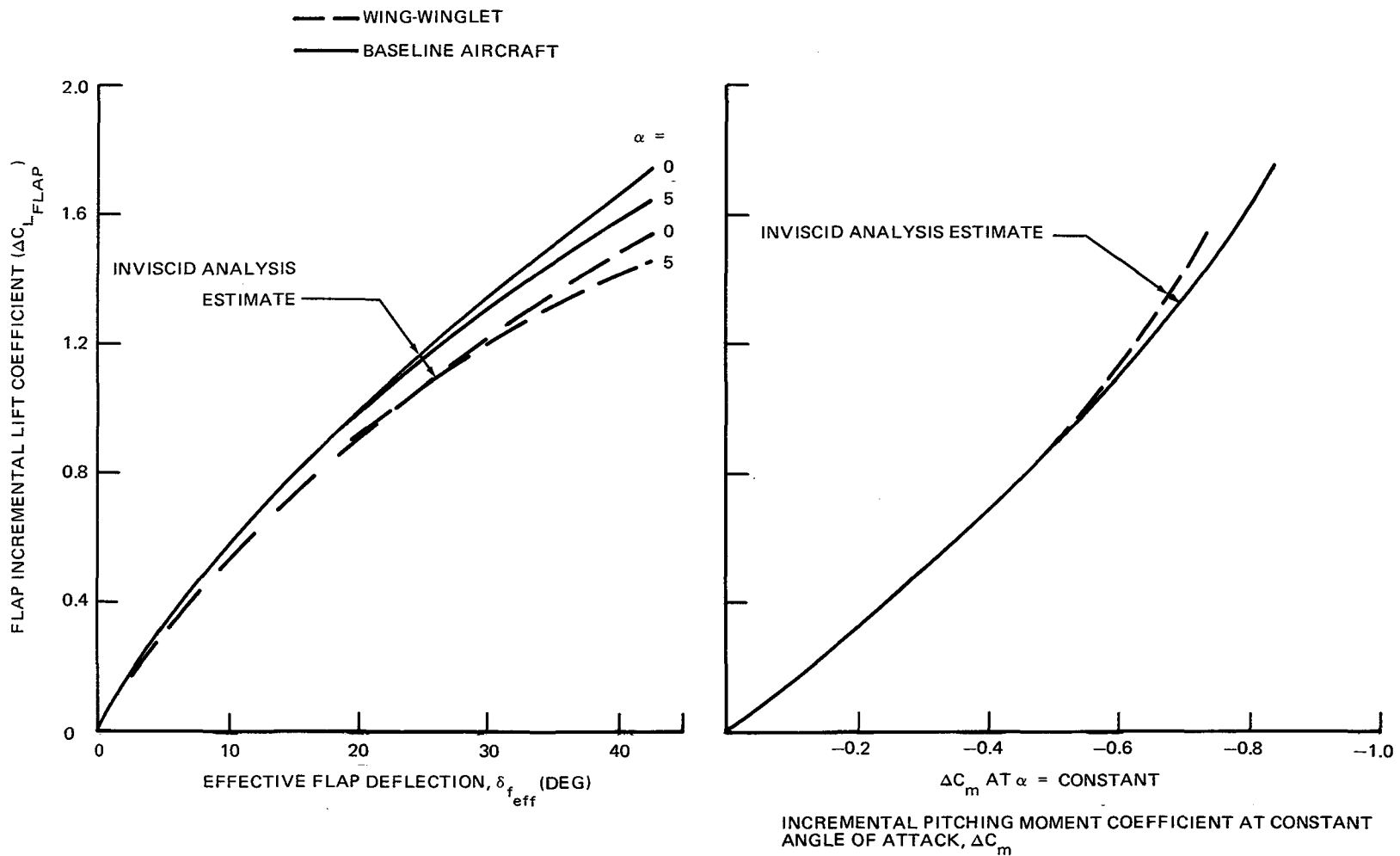
FIGURE 22. COMPARISON OF FLAP EFFECTIVENESS AND PITCHING MOMENTS OF BASELINE AND WING-WINGLET AIRCRAFT

calculates the total fuel required to complete the input mission profile. The weights subprogram is then called to calculate the operator's empty weight for the particular wing area, engine size, and takeoff gross weight. Available payload (takeoff gross weight minus operator's empty weight minus total fuel required) is then compared with the design payload required. A new takeoff gross weight is selected and the mission calculations are repeated until the correct payload is achieved. When the mission balance is complete, the program calculates approach speed at the mission landing weight.

Program inputs include drag data in the form of efficiency factor, parasite drag equivalent flat plate area, and compressibility drag. Additional aero-dynamic input data specify the lift coefficient at minimum speed and the buffet lift coefficient. The aircraft operating empty weight is provided to the sizing analysis in the form of weight equations expressed in terms of the independent variables of wing area and takeoff gross weight. Engine characteristics were supplied in tabular form with net thrust and fuel flow as a function of Mach number, pressure altitude, and temperature for maximum climb, maximum cruise, and at flight idle power settings. Additionally, engine fuel flow for cruise rating is also stored as a function of (partial) power settings.

The aircraft was optimally sized within the analysis program by determining the takeoff gross weight and wing area needed to meet approach speed and initial cruise altitude requirements for the specified design range and payload. Results of the sizing process are summarized in Table 12 for both the baseline and wing-winglet aircraft. Table 12 indicates that the wing-winglet aircraft has a larger wing area but is lighter than the baseline aircraft.

Table 12

SIZING AND PERFORMANCE RESULTS FOR BASELINE AND WING-WINGLET AIRCRAFT

		Baseline Aircraft	Wing-Winglet Configuration
Sizing Input	Engines	GE CF6-45	GE CF6-45
	No.	2	2
	Sea Level Static Thrust/Engine	200.16 kN (45,000 lb)	200.16 kN) (45,000 lb)
	Passengers	230	230
	Design Payload	21,390 kg (47,150 lb)	21,390 kg (47,150 lb)
	Design Range	4855 km (2620 n mi)	4855 km (2620 n mi)
	Cruise Mach	0.80	0.80
Sizing Results	Maximum Takeoff Gross Weight	133,825 kg (295,035 lb)	132,473 kg (292,055 lb)
	Operating Empty Weight	79,255 kg (174,728 lb)	78,573 kg (173,270 lb)
	Operational Landing Weight	106,032 kg (233,762 lb)	105,283 kg (232,111 lb)
	Landing Flaps	20/10 deg	20/10 deg
	Approach Speed	241 km/hr (130 kn)	241 km/hr (130 kn)
	Initial Cruise Altitude	10,394 m (34,100 ft)	10,485 m (34,400 ft)
	Takeoff Field Length at SL, 84°F	2286 m (7500 ft)	2362 m (7750 ft)
	Wing Area	208 sq m (2242 sq ft)	209 sq m (2255 sq ft)
	Parasite Drag Equivalent Flat Plate Area	3.880 sq m (41.776 sq ft)	3.808 sq m (40.985 sq ft)
	Aspect Ratio	10.85	8.24
Mission Results	750-n mi Mission		
	Block Time	2.021 hr	2.022 hr
	Block Fuel	8275.7 kg (18,245 lb)	8151.9 kg (17,972 lb)
	Constant Altitude	11,278 m (37,000 ft)	11,278 m (37,000 ft)

Subsequent to the sizing calculation, the flight characteristics of the resized aircraft were then determined. The flight mission profile is specified in Table 2. The block data results for baseline and resized wing-winglet aircraft are given in the lower part of Table 13. These block data were employed in the direct operating cost calculations.

Table 13

INPUTS TO DIRECT OPERATING COSTS EVALUATION

Input	Baseline	Wing-Winglet
Engine		
Model	GE CF6-50	GE CF6-50
Number	2	2
Sea Level Static Thrust	200.16 kN/engine (45,000 lb/engine)	200.16 kN/engine (45,000 lb/engine)
Extra Derate	25 percent	25 percent
Weight		
Maximum Takeoff	295,035 lb	292,055 lb
Cost Weight	138,780 lb	137,410 lb
Prices		
Total Aircraft	$23,902,000	$23,842,000
Engine	$1,873,000	$1,873,000
Fuel	$0.13/liter ($0.50/gallon)	$0.13/liter ($0.50/gallon)
Capacity		
Passenger Seats	230	230
Cockpit Crew	3	3
Block Data		
Stage Length	1389 km (750 n mi)	1385 km (750 n mi)
Block Fuel	8276 kg (18,245 lb)	8152 kg (17,972 lb)
Block Time	2.021 hr	2.022 hr
Flight Time	1.888 hr	1.889 hr

Direct Operating Costs Evaluation

The direct operating costs (DOC) were estimated for both the baseline and wing-winglet aircraft by employing modified versions of the Air Transport Association DOC equations which are outlined in Reference 14. The modifications consist of updating the equations to reflect recent operating experience and current prices. DOCs were calculated in 1978 dollars with a fuel cost of 13 cents per liter (50 cents per gallon). Maintenance cost estimates were based on the first 5 years average since this period is generally of principal interest to the airline operators. An aircraft productivity of 1,852,000 kilometers (1,000,000 nautical miles) per year was assumed. Additionally, a 16-year depreciation period with a residual value of 0.16 of the original cost was employed. Development costs were estimated to be $754,260,000 for the baseline aircraft and $755,150,000 for the wing-winglet configuration. Even though the latter number includes $5,000,000 dollars for winglet development, the wing-winglet development expense is estimated to be only slightly greater than the baseline expense since the wing-winglet aircraft is smaller in size than the baseline aircraft. Since the development costs were distributed over 400 aircraft (with a 20-percent pretax profit), the impact of development costs on the relative price of the two aircraft is relatively insignificant.

The DOCs for both the baseline and wing-winglet aircraft are given in
Table 14 for the mission of Table 2. Comparison of the DOC totals for the two
aircraft indicates a 0.7-percent lower DOC for the optimized wing-winglet air-
craft than for the conventional wing aircraft. This DOC increment is considered

Table 14
RESULTS OF DIRECT OPERATING COSTS CALCULATION
(Mission Given in Table 2)

Component	Cost Per Flight ($) Baseline	Cost Per Flight ($) Wing-Winglet
Cockpit Crew	746.32	744.86
Depreciation		
- Airframe	918.36	915.62
- Engines	197.54	197.54
Insurance	134.45	134.11
Landing Fee	221.28	219.04
Airframe Maintenance		
- Labor	307.29	306.24
- Material	126.60	126.35
Engine Maintenance		
- Labor	88.52	88.55
- Material	109.39	109.43
Fuel	1361.57	1341.19
Total	4211.32	4182.95
Cost Per Nautical Mile	$ 5.6151	$ 5.5773
Cost Per Seat Mile	$ 0.0244	$ 0.0242

to be significant, and indicates that development of the optimized wing-winglet concept warrants further investigation. The wing-winglet configuration consumed 1.5 percent less fuel than the baseline aircraft for the specified mission. In fact, fuel consumption reduction was responsible for a substantial portion (72 percent) of the wing-winglet aircraft DOC benefit. The wing-winglet concept therefore warrants further development in view of the energy saving potential.

CONCLUSIONS AND RECOMMENDATIONS

This study of an integrated wing and winglet lift system applied to a medium-range advanced commercial aircraft has yielded favorable indications of the advantage of the wing-winglet system. This advantage is reflected in significantly lower direct operating costs and includes substantial energy savings. DOC calculations indicate that the present optimized wing-winglet configuration can complete a typical 1389-kilometer (750-nautical-mile) mission at a 0.7 percent lower cost than the comparable conventional wing aircraft. Most of the reduction in operating costs results from lower fuel consumption.

Apart from these results, the study concludes that the selection of the optimum wing-winglet design was strongly influenced by flutter requirements. Although the final wing-winglet configuration was predicted to have zero flutter penalty, any significant revision in flutter performance of the wing-winglet system could certainly impact the configuration definition, and perhaps affect the advantage described above. Therefore, additional investigation of the flutter characteristics of wing-winglet systems is recommended in order to confirm their potential benefits.

Additionally, although no specific problems were identified during the wing-winglet high-lift-system analysis, some uncertainty in achievable low-speed performance, resulting from lack of experience with winglet high-lift systems, has been identified. Consequently, further investigation of low-speed winglet aerodynamics is recommended.

Under the stated design rules and guidelines, the wing-winglet combination provided a lighter lift system than a comparably performing high-aspect-ratio conventional wing. However, this result cannot necessarily be generalized to all aircraft configurations.

In conclusion, the study shows that estimated DOC and fuel savings are of sufficient magnitude to sustain interest in further development of an aircraft designed with a winglet from its inception.

REFERENCES

1. Mechtly, E. A., "The International System of Units — Physical Constants and Conversion Factors," NASA SP-7012, 1973.

2. Whitcomb, R. T., "A Design Approach and Selected Wind Tunnel Results at High Subsonic Speeds for Wing-Tip Mounted Winglets," NASA TN D-8260, 1976.

3. Flechner, S. G., Jacobs, P. F. and Whitcomb, R. T., "A High Subsonic Speed Wind-Tunnel Investigation of Winglets on a Representative Second-Generation Jet Transport Wing," NASA TN D-8264, 1976.

4. Jacobs, P. F., Flechner, S. G., and Montoya, L. C., "Effect of Winglets on a First-Generation Jet Transport Wing I, II and III," NASA TN D-8473, TN D-8474, and TN D-8478, 1977.

5. Taylor, A. B., "Advanced Aerodynamics and Active Controls for a Next Generation Transport," NASA Conference Publication 2036, Part II, CTOL Transport Technology, 1978.

6. Gilkey, R. D., "Final Report — Design and Wind Tunnel Tests of Winglets on a DC-10 Wing," Douglas Aircraft Company Report ACEE-05-FR-8423, July 1978.

7. Tulinius, J., Gloss, B., and Thomas, J., Unpublished Numerical Method for Specification of Span Load Distribution of Arbitrary Lift Systems with Minimum Induced Drag and Moment Constraints. Described in: Tulinius, J. R., and Margason, R. J., "Aircraft Aerodynamic Design and Evaluation Methods," AIAA Paper No. 76-15, 1976.

8. Lundry, J. L., "A Numerical Solution for the Minimum Induced Drag, and the Corresponding Loading of Nonplanar Wings," Douglas Aircraft Company Report DAC-66900, 1968.

9. Goldhammer, M. I., "A Lifting Surface Theory for the Analysis of Nonplanar Lifting Systems," AIAA Paper No. 76-16, 1976.

10. Anonymous, "Airworthiness Standards for Transport Category Airplanes," Federal Aviation Regulations, Part 25, 1978.

11. Giesing, J. P., Kalman, T. P., Rodden, W. P., "Subsonic Unsteady Aerodynamics for General Configurations," AIAA Paper No. 72-26, 1972.

12. Clutter, D. W., "Charts for Determining Skin-Friction Coefficients on Smooth and on Rough Flat Plates at Mach Numbers Up to 5.0 With and Without Heat Transfer," Douglas Aircraft Company Report ES 29074, 1959.

13. Finck, R. D., "USAF Stability and Control DATCOM," Contract AF 33(616)-6460, 1975.

14. Anonymous, "Standard Method of Estimating Comparative Direct Operating Costs of Turbine Powered Transport Airplanes," Air Transport Association of America, 1967.

1. Report No. NASA CR-159156	2. Government Accession No.	3. Recipient's Catalog No.
4. Title and Subtitle Application of an Optimized Wing-Winglet Configuration to an Advanced Commercial Transport		5. Report Date November 1979
		6. Performing Organization Code
7. Author(s) C. A. Shollenberger		8. Performing Organization Report No. ACEE-06-FR-9661 (Rev. 11-79)
9. Performing Organization Name and Address Douglas Aircraft Company McDonnell Douglas Corporation 3855 Lakewood Boulevard Long Beach, California 90846		10. Work Unit No.
		11. Contract or Grant No. NAS1-14744
12. Sponsoring Agency Name and Address National Aeronautics and Space Administration Washington, D.C. 20546		13. Type of Report and Period Covered Contractor Report
		14. Sponsoring Agency Code

15. Supplementary Notes
Project TRCO, D. L. Maiden, Energy Efficient Transport Project,
NASA Langley Research Center, Hampton, Virginia 23665

16. Abstract

This report presents the design of an aircraft which from the initial conceptual stages employs an integrated wing and winglet lift system. Comparison was made with a conventional baseline configuration employing a high-aspect-ratio super-critical wing. An optimized wing-winglet combination was selected from four proposed configurations for which aerodynamic, structural, and weight character-istics were evaluated. Each candidate wing-winglet configuration was constrained to the same induced drag coefficient as the baseline aircraft. The selected wing-winglet configuration was resized for a specific medium-range mission requirement, and operating costs were estimated for a typical mission. Study results indicated that the wing-winglet aircraft was lighter and could complete the specified mission at less cost than the conventional wing aircraft. These indications were sensitive to the impact of flutter characteristics and, to a lesser extent, to the performance of the high-lift system. Further study in these areas is recommended to reduce uncertainty in future development.

| 17. Key Words (Suggested by Author(s))
Winglets
Wing-tip extensions
Cruise drag reduction
Wing bending moment
Aircraft design | 18. Distribution Statement

FEDD Distribution | | |
| 19. Security Classif. (of this report)
Unclassified | 20. Security Classif. (of this page)
Unclassified | 21. No. of Pages
71 | 22. Price*
 |

*Available: NASA's Industrial Applications Centers